Modeling the impact of riverine DON removal by marine bacterioplankton on primary production in the Arctic Ocean

[1]Vincent Le Fouest

[2]Manfredi Manizza

[3]Bruno Tremblay

[4]Marcel Babin

[1]Littoral Environnement et Sociétés, UMR 7266, Université de La Rochelle, La Rochelle, France

[2]Geosciences Research Division, Scripps Institution of Oceanography, University of California San Diego, La Jolla, CA, USA

[3]Department of Atmospheric and Oceanic Sciences, McGill University, Montreal, QC, Canada

[4]Takuvik Joint International Laboratory, Université Laval (Canada) & Centre National de la Recherche Scientifique (France), Département de Biologie, Québec, QC, Canada

Abstract

The planktonic and biogeochemical dynamics of the Arctic shelves exhibit a strong variability in response to Arctic warming. In this study, we employ a biogeochemical model coupled to a pan-Arctic ocean-sea ice model (MITgcm) to elucidate on the processes regulating the production of phytoplankton (PP), bacterioplankton (BP), and their interactions. The model explicitly simulates and quantifies the contribution of usable dissolved organic nitrogen (DON) drained by the major circum-Arctic rivers on PP and BP in a scenario of melting sea ice (1998–2011). Model simulations suggest that on average between 1998 and 2011, the removal of usable RDON by bacterioplankton is responsible for a ~26% increase in the annual BP for the whole Arctic Ocean. With respect to total PP, the model simulates an increase of ~8% on an annual basis and of ~18% in summer. Recycled ammonium is responsible for the PP increase. The recycling of RDON by bacterioplankton promotes higher BP and PP but there is no significant temporal trend in the BP:PP ratio within the ice-free shelves over the 1998-2011 period. This suggests no significant evolution in the balance between autotrophy and heterotrophy in the last decade with a constant annual flux of RDON into the coastal ocean. Although, changes in RDON supply and further reduction in sea ice cover could potentially alter this delicate balance.

1. Introduction

In response to the polar amplification of global climate change, air temperature in the lower atmosphere is increasing twice as fast in the Arctic as in temperate regions. By the end of the century, model projections suggest an average increase of the surface air temperature of 3.7°C relative to 1981-2000 (ACIA report, 2005). In response to Arctic warming, plankton production and the biogeochemistry of the Arctic Ocean (AO) is rapidly evolving. Changes in phytoplankton communities (Li et al., 2009) as well as their phenology in spring (Kahru et al., 2011) and fall (Ardyna et al., 2014) are being observed. Overall, the AO tends to be more productive (Bélanger et al., 2013) and is taking up more atmospheric carbon dioxide (1996-2007; Manizza et al., 2013). In the long term, model projections suggest an increase of spatially integrated primary production (PP) by the end of the 21st century (Vancoppenolle et al., 2013).

The AO is the basin the most influenced by continental freshwater. It receives 10% of the freshwater that flows into the global ocean, but represents only 1% of the global ocean volume (Opshal et al., 1999). Circum-Arctic rivers are potentially a significant source of inorganic nutrients and organic matter for shelf seas (Le Fouest et al., 2013; Tank et al., 2012). 10 % of the global riverine inputs of organic carbon are conveyed into the AO (Rachold et al. 2004). This fraction is projected to increase in the near future due to the accelerated thawing of permafrost (Frey et al., 2007). This pool of organic matter enters the carbon cycle but little is known about its fate and pathways within the plankton ecosystem in Arctic waters prior to being exported into the Atlantic Ocean.

Bacterioplankton is a major biological component involved in the degradation and mineralization of dissolved organic matter in Arctic waters (Retuerta-Ortega et al., 2012a). It can significantly

affect fate and distribution of organic matter within the entire water column (Bendsten et al., 2002) as well as the microbial food web activity through the assimilation of remineralized nitrogen. However, the contribution of Arctic bacterioplankton to plankton production in the context of Arctic warming remains unknown. Despite the fact that the AO basin now acts as a sink for atmospheric carbon dioxide (1996-2007; Manizza et al., 2013), the balance between autotrophy and heterotrophy may change in the future based on observations of enhanced stratification of the water column (Li et al., 2009), increased sea temperature (Timmermans et al., 2014; Steele et al., 2008), which acts as a key driver of Arctic bacterioplankton metabolism (Piontek et al., 2014; Bendsten et al., 2002), and changes in the riverine inputs of nutrients due to an increase in freshwater discharge (Shiklomanov and Lammers, 2011). In near-shore AO waters, riverine inputs already sustain part of the bacterial activity (e.g. Vallières et al., 2008).

Using a relatively simple biogeochemical modeling approach, Tank et al. (2012) shed light on the potential impact of riverine nutrients inputs on the PP of the AO. In the present study, we propose building on the static view provided by the work of Tank et al. (2012) by explicitly modeling the effect of the interactions between riverine dissolved organic nitrogen (RDON) and bacterioplankton. The objective is to use a pan-Arctic ocean-sea ice coupled model to quantify the contribution of usable RDON processed by marine bacterioplankton on the production of both bacterioplankton and phytoplankton in a scenario of melting sea ice over the period 1998-2011.

2. Material and Methods

2.1 The physical model

78 We used the MIT General Circulation model (MITgcm) (Marshall et al., 1997) coupled with a
79 sea-ice model. The model is configured on a "cubed-sphere" grid encompassing the Arctic
80 domain with open boundaries at ≈55°N in the Atlantic and Pacific sectors. Prescribed boundary
81 conditions for potential temperature, salinity, flow, and sea-surface elevation are provided from
82 previous integrations of a global configuration of the same model (Menemenlis et al., 2005). The
83 grid has a variable horizontal resolution with an average mesh of ~18 km. The mesh resolves
84 major Arctic straits, including many of the channels of the Canadian Archipelago. The sea-ice
85 and fluid dynamics equations are solved on the same horizontal mesh. The 50-level vertical grid
86 is height based, varying from 10 m thick near the surface to ~450 m at a depth of ~6 km.
87 Bathymetry is derived from the U.S. National Geophysical Data Center (NGDC) two-minute
88 global relief data set (ETOPO2), which uses the International Bathymetric Chart of the Arctic
89 Ocean (IBCAO) product for Arctic bathymetry (Jakobsson et al., 2008). The ETOPO2 data is
90 smoothed to the model's horizontal mesh and mapped to the ocean's vertical levels using a
91 "lopped cell" strategy (Adcroft et al., 1997), which permits an accurate representation of the
92 ocean bottom boundary.

93 The ocean model's hydrography is initialized with observations taken from the Polar Science
94 Center Hydrographic Climatology (PHC) 3.0 database (Steele et al., 2001). Initial sea-ice
95 distributions are taken from the pan-Arctic Ice-Ocean Modeling and Assimilation System data
96 sets (Zhang and Rothrock, 2003). Atmospheric forcings (10 m surface winds, 2 m air
97 temperature and humidity, and downward longwave and shortwave radiation) are taken from the
98 six-hourly data sets of the Japanese 25-year ReAnalysis (JRA-25) (Onogi et al., 2007). Monthly
99 mean estuarine fluxes of freshwater are based on the Arctic Runoff database (Lammers et al.,
100 2001; Shiklomanov et al., 2000). The sea-ice component of the coupled model follows the

viscous-plastic rheology formulation of Hibler (1979) with momentum equations solved implicitly on a C-grid (Arakawa and Lamb, 1977) using a procedure based on Zhang and Hibler (1997). Fluxes of momentum into ice due to the overlying atmospheric winds and momentum fluxes between sea-ice and the ocean are calculated by solving for the momentum balance at each surface grid column (Hibler and Bryan, 1987). This model configuration was previously used to study the Arctic freshwater budget (Condron et al., 2009). Modeling studies of Condron et al. (2009) compared to observations by Serreze et al. (2006) concluded that this model configuration is able to realistically represent the freshwater budget of the AO, including the import and export of freshwater from the Bering and Fram straits and from the Canadian Archipelago.

2.2 The riverine DON (RDON) discharge

To realistically represent the RDON flux in the AO in our biogeochemical model we follow the approach adopted by Manizza et al. (2009), which is based on seasonally-explicit regression relationships. These relationships use co-variations between water yield and dissolved organic carbon (DOC) concentrations in circum-Arctic rivers to define RDOC monthly-averaged fluxes for 10 regions in the pan-Arctic domain. These regions are the Barents Sea, Kara Sea, Laptev Sea, East Siberian Sea, Chukchi Sea, Bering Strait, Beaufort Sea, Canadian Archipelago, Hudson Bay, and Hudson Strait using published watershed areas and seasonal water runoff (Lammers et al., 2001). The approach uses empirical relationships quantifying the co-variation between discharge and riverine DOC (RDOC) to scale the Lammers et al. (2001) discharge estimates into estimates of RDOC export. Estimates of RDOC export for December–March, April–July, and

August–November were divided into monthly bins according to measured distributions of RDOC export for those months in Arctic rivers. For each season, [RDOC]-discharge relationships were developed. North American and Eurasian rivers were considered separately. Data from the Yukon, Mackenzie, and Kuparuk rivers were used to define a runoff-[RDOC] relationship for drainage areas in North America, and data from the Ob', Yenisey, and Lena rivers were used to define a runoff-[RDOC] relationship for drainage areas in Eurasia. RDOC for the Yenisey, Ob', Lena, and Mackenzie were collected as part of the Pan-Arctic River Transport of Nutrients, Organic Matter, and Suspended Sediments (PARTNERS) project (McClelland et al., 2008). RDOC concentrations for the Kuparuk River were collected as part of the NSF Study of the Northern Alaska Coastal System (SNACS, http://www.arcus.org/arcss/snacs/index.php). In all cases, discharge data were acquired from ArcticRIMS (http://rims.unh.edu/). Recent sampling efforts on these rivers have provided exceptional seasonal coverage (McClelland et al., 2008) and the total annual discharge of RDOC in the model is 37.7 TgC yr^{-1}, which is consistent with the estimate of Raymond et al. (2007). To initialize the model, we used the three-dimension RDOC field obtained from the 3-decade integration of the model by Manizza et al. (2009). After that time, RDOC distributions are relatively steady, because the flushing time for tracers through the surface waters of the basin is on the order of a decade. RDOC was converted into nitrogen currency (RDON) using a molar C:N ratio of 40:1 (Tank et al., 2012.; Köhler et al., 2003). We assume that 15% of the RDON entering the model at river grid cells is usable by bacterioplankton (e.g. Wickland et al., 2012).

2.3 The biogeochemical model

We couple to the MITgcm physical model a biogeochemical model that explicitly represents the plankton ecosystem dynamics. The biogeochemical model is improved from previous applications in sub-Arctic (Le Fouest et al., 2005; 2006) and Arctic waters (Le Fouest et al., 2011; 2013b). In the model, nitrogen is the currency and it includes 10 compartments (i.e., nine in the pelagic domain + RDON that couples the marine and terrestrial cycling of nitrogen), chosen according to the ecosystem structure observed in the AO. Phytoplankton is size-fractionated into large (> 5 μm) and small (< 5 μm) phytoplankton (LP and SP, respectively). These two compartments encompass the major phytoplankton groups relevant for plankton dynamics and biogeochemistry in the Arctic waters (e.g. Li et al., 2009; Coupel et al., 2012). The two zooplankton compartments represent large (LZ, mainly copepods) and small (SZ, protozooplankton) organisms. Dissolved inorganic nutrients are nitrate (NO_3) and ammonium (NH_4). Detrital (i.e. produced by the biogeochemical model components) particulate and dissolved organic nitrogen (dPON and dDON, respectively) close the nitrogen cycle. Bacterioplankton (BACT) are explicitly represented following the model of Fasham et al. (1990). They grow on NH_4, dDON and on the usable fraction of RDON (see appendix for details). LP and SP growth depends on light, NO_3 and NH_4 availability according to the Liebig's law of the minimum. LZ graze on LP and SZ, whereas SZ graze on SP and BACT. Fecal pellets and LP basal mortality fuel the dPON pool. The dDON pool is made of unassimilated nitrogen resulting from SZ grazing, SP, SZ and BACT basal mortality and dPON fragmentation. BACT release, LZ excretion and unassimilated nitrogen resulting from SZ grazing are the sources of NH_4 in the model. NH_4 is converted into NO_3 through the nitrification process. For phytoplankton, nitrogen is converted into carbon using the Redfield carbon to nitrogen (C:N) molar ratio (106:16; Redfield et al., 1963) and into Chl using variable C:Chl mass ratios computed according to a

168 modified version of the phytoplankton photoacclimation model of Cloern et al. (1995). The
169 plankton biogeochemical model (Fig. 1) is fully detailed in the appendix. Differential equations
170 are given in Table 1, whereas biological parameters are given in Table 2.

171 Nitrate data used for the model initialization are from the World Ocean Atlas 2005 (National
172 Oceanographic Data Centre, 2006). LP and SP are assigned a constant field over the model grid
173 (0.2 mmol N m^{-3} and 0.002 mmol N m^{-3} in the top eighth layers and below, respectively) (e.g.
174 Sherr et al., 2003; Ducklow, 1999, Taniguchi, 1999). Same conditions are imposed for BACT
175 (e.g. Sherr et al., 2003; Ducklow, 1999). LZ and SZ are assigned a constant field over the model
176 grid (0.1 mmol N m^{-3} and 0.001 mmol N m^{-3} in the top eighth layers and below, respectively)
177 (e.g. Sherr et al., 2003, Taniguchi, 1999). Same conditions are imposed a priori for dPON. A
178 value of 1 mmol N m^{-3} of NH_4 (e.g. Kristiansen et al., 1994) and dDON (e.g. Charria et al.,
179 2008) is imposed at each grid cell. Boundary conditions at the North Atlantic and North Pacific
180 sectors are data from the World Ocean Atlas 2005 (NODC, 2006) for NO_3, and null for the
181 remaining 9 biogeochemical tracers. Apart from RDON, there are no riverine inputs for the
182 remaining 9 biogeochemical tracers.

183

184 **2.4 Coupled model integrations**

185 The model is spun up by repeating the January 1980-December 1989 decade twice. It is
186 thereafter initialized with the physical and biogeochemical fields obtained from December 31,
187 1989 to run the 1990-2011 time period. Two simulations are then carried out: without usable
188 RDON removal by bacterioplankton (our control run, hereafter CTRL run) and with usable
189 RDON removal by bacterioplankton (hereafter RIV run). The difference between the two

simulations provides information on the potential impact of the interactions between bacterioplankton and usable RDON on bacterioplankton production (BP), nutrients regeneration, and ultimately primary production (PP) in the Arctic basin.

3. Results

3.1 Primary production

Shelf seas influenced the least by riverine inputs of RDON show comparable simulated annual rates of total PP in the CTRL and RIV runs (Fig. 2). In the Barents Sea, simulated PP averaged over 1998-2011 reaches up to ~80 gC m^{-2} yr^{-1}, in line with previous remote sensing estimates (up to 70-80 gC m^{-2} yr^{-1} in average over 1998-2010; Bélanger et al., 2013). In the central Chukchi Sea, simulated PP lies between 50-80 gC m^{-2} yr^{-1}, in agreement with the observed range (15-80 gC m^{-2} yr^{-1} in average over 1998-2007; in Bélanger et al., 2013).

The largest differences in total PP between the two runs are found in the river-influenced Eurasian seas (East-Siberian Sea, Laptev Sea, and Kara Sea) (Fig. 2). In the CTRL run, maximum simulated PP rates reach ~30 gC m^{-2} yr^{-1}, which is more than 3-fold lower than satellite-derived and in-situ estimates that can exceed 100 gC m^{-2} yr^{-1} (Bélanger et al., 2013; Codispoti et al., 2013; Sakshaug, 2004). In contrast, PP rates simulated in the RIV run (80-90 gC m^{-2} yr^{-1}) show a better agreement with observations.

The increase of the 1998-2011 averaged annual PP in the RIV run relative to the CTRL run is due to the increase of NH_4-supported PP (Figs. 3d, 3e and 3f). In contrast, overall, new PP remains unaffected by the bacterial use of RDON (Figs. 3a, 3b and 3c). In the Kara Sea, Laptev

211 Sea, East-Siberian Sea, and Beaufort Sea, simulated new PP is mostly <20 gC m^{-2} yr^{-1}, in
212 agreement with previously estimated rates (<17 gC m^{-2} yr^{-1}; Sakshaug, 2004). New PP rates
213 simulated by the model in the more productive areas are also in line with Sakshaug's estimated
214 rates. In the Chukchi Sea, new PP generally lies in the 10-30 gC m^{-2} yr^{-1} range and reaches >100
215 gC m^{-2} yr^{-1} at the sea opening (5-160 gC m^{-2} yr^{-1}; Sakshaug, 2004). Simulated new PP is up to
216 ~70 gC m^{-2} yr^{-1} in the Barents Sea, close to the value given by Sakshaug (up to 100 gC m^{-2} yr^{-1};
217 2004). In the Greenland and Labrador Seas, the simulated new PP rates are ~50 gC m^{-2} yr^{-1} and
218 ~30 gC m^{-2} yr^{-1}, respectively (40-45 gC m^{-2} yr^{-1}; Sakshaug, 2004).

219 Direct estimates of NH_4-supported PP based on measurements are rare in Arctic coastal waters.
220 Nevertheless, they can be crudely derived by subtracting new PP from total PP estimated by
221 Sakshaug (2004). In the Eurasian and North American shelves, NH_4-supported PP in the CTRL
222 run is <10 gC m^{-2} yr^{-1} (Fig. 3d) overall. This is low relative to the rates derived from Sakshaug's
223 data, which would range between ~25 gC m^{-2} yr^{-1} and ~40 gC m^{-2} yr^{-1}. By contrast, in the RIV
224 run, rates simulated in offshore shelf waters are ~10-30 gC m^{-2} yr^{-1}. However, closer to the coast,
225 local rates reach 40-50 gC m^{-2} yr^{-1} (Laptev Sea) and 70-80 gC m^{-2} yr^{-1} (Kara Sea) (Fig. 3e).

226 Averaged over 1998-2011, the total PP simulated by the model and integrated over the whole
227 AO is 662±91 TgC yr^{-1} in the CTRL run and 717±95 TgC yr^{-1} in the RIV run. These values are
228 within the range of previously reported rates based on remote sensing or in-situ data (385-1008
229 TgC yr^{-1}, Bélanger et al., 2013; Codispoti et al., 2013; Hill et al., 2013; Arrigo and van Dijken,
230 2011). Between the two model runs, the annual total PP increased by ~8%, on average, between
231 1998 and 2011. In September-October, when the simulated sea ice concentration reaches its
232 seasonal minimum, the annual total PP increase is more than twice this value (~18%, on
233 average).

234

235 **3.2 Bacterioplankton activity**

236 The PP increase is tightly linked to a higher bacterioplankton activity that promotes RDON
237 recycling into nutrients usable by both phytoplankton and bacterioplankton. The
238 bacterioplankton biomass (BB), integrated between the sea surface and 50 m and averaged over
239 April to June (spring) and July to September (summer), is shown in figure 4. As for PP, the
240 Barents and Chukchi Seas show comparable levels of BB in CTRL and RIV runs. In the Chukchi
241 Sea, the BB simulated in spring (<100-250 mgC m^{-2}; Figs. 4a and 4b) overlaps with the
242 measured range (222-358 mgC m^{-2}; Kirchman et al., 2009). It is similar in summer, when
243 simulated (~100 mgC m^{-2} to >800 mgC m^{-2}; Figs. 4d and 4e) and measured BB levels (250-507
244 mgC m^{-2}; Kirchman et al., 2009; Steward et al., 1996) are higher than in spring. In the Barents
245 Sea, the simulated BB increases from <100 mgC m^{-2} in spring to <250 mgC m^{-2} in summer,
246 falling within the measured range (from ~80 mgC m^{-2} in spring to ~400 mgC m^{-2} in summer, on
247 average; Sturluson et al., 2008). In the highly river-influenced shelf seas, the two runs show
248 notable differences in their simulated BB (Figs. 4 c and 4f). In the central part of the Kara Sea,
249 influenced by the Ob' and Yenisey River plumes, BB measured in late summer along a South-
250 North transect from the Yama Peninsula to the Novaya Zemlya island is reported to range
251 between ~0.1 mgC m^{-3} and 7 mgC m^{-3} (Sazhin et al., 2010). For the same time period and along
252 a comparable transect, simulated values of BB are <2 mgC m^{-2} in the CTRL run. However, in the
253 RIV run, BB increases up to ~6-7 mgC m^{-3} to match the values measured by Sazhin et al. (2010).

254 The depth-integrated (0-50 m) bacterioplankton production (BP) simulated in both the CTRL and
255 RIV runs in summer in the Chukchi Sea (<280 mgC m^{-2} d^{-1}) is consistent with measurements

256 reported for the same season (5-301 mgC m^{-2} d^{-1}; Kirchman et al., 2009; Rich et al., 1997;
257 Steward et al., 1996). In the Beaufort Sea, influenced by the Mackenzie River plume, simulated
258 BP is lower than ~6 mgC m^{-2} d^{-1} in the CTRL run, which is much below measurements made
259 within the area (25-68 mgC m^{-2} d^{-1}; Ortega-Retuerta et al., 2012a; Vallières et al., 2008). By
260 contrast, in the RIV run, simulated BP (<30 mgC m^{-2} d^{-1}) approaches the lower range of
261 observations. Similarly, BP simulated in the CTRL run for the Kara Sea (<30 mgC m^{-2} d^{-1}) does
262 not exceed the first mid-range of measurements given by Meon and Amon (2004) (12-79 mgC
263 m^{-2} d^{-1}; 2004). In the RIV run, the simulated BP (~4-90 mgC m^{-2} d^{-1}) overlaps the measured
264 range (12-79 mgC m^{-2} d^{-1}; Meon and Amon, 2004) to reach up to 120 mgC m^{-2} d^{-1} locally. This
265 result is consistent with enrichment experiments conducted with surface oceanic water sampled
266 in the Beaufort Sea that showed a 43% increase of BP when Mackenzie River water was
267 included in samples (see Ortega-Retuerta et al., 2012a).

268 Averaged over 1998-2011, the total BP simulated by the model and integrated over the whole
269 AO is, on average, 26% higher in the RIV run (68±9 TgC yr^{-1}) than in the CTRL run (54±8 TgC
270 yr^{-1}). Bacterioplankton recycle RDON into nutrients that can be used by both phytoplankton and
271 bacterioplankton, hence promoting their growth. In addition, bacterioplankton and small
272 phytoplankton are grazed by microzooplankton that, in turn, are grazed by mesozooplankton.
273 More organic matter is channeled towards the upper trophic levels, a flow that also contributes to
274 fueling the dDON and NH_4 pools through recycling. By enabling the removal of RDON by
275 bacterioplankton in the biogeochemical model, the biomass of microzooplankton and
276 mesozooplankton, averaged over 1998-2011, increased by ~16.1% and 43.6%, respectively.

277

3.3 The bacterioplankton production versus primary production ratio (BP:PP)

The BP:PP ratio is computed over the AO shelf, delimited here by the 200 m isobaths, for ice-free waters (i.e. with less than 30% of ice cover). On average for the 1998-2011 period, the simulated BP:PP ratio is 0.19±0.02 in the CTRL run and 0.21±0.01 in the RIV run. These values lie within the range observed in open (0.02; Kirchman et al., 2009) and coastal waters (0.37-0.43; Ortega-Retuerta et al., 2012a; Garneau et al., 2008). When looking at the temporal evolution of BP:PP in the RIV run (Fig. 5), the model simulates a significant increase of PP ($r = 0.57$, $p<0.05$) and BP ($r = 0.63$, $p<0.05$) between 1998 and 2011, with a production maximum simulated in 2007, the year showing the higher sea ice minimum. However, there is no evidence of a significant temporal trend of BP:PP ($r = -0.09$, $p>0.05$) over 1998-2011. This result suggests that, with a constant annual flux of RDON into the coastal AO, the significant increase in simulated BP in the model is not high enough to promote a higher contribution of heterotrophy with respect to autotrophy within the upper water column.

4. Discussion

The coupled model suggests that NH_4 produced from the remineralization of RDON by the microbial food web contributed ~8% to annual pan-Arctic PP over the 1998-2011 period. This is about twice the value given in the study by Tank et al. (2012) that, in addition to RDON, accounted for the contribution of riverine inorganic nutrients as well as of the photochemical transformation of RDON into NH_4. In our coupled model, the uptake of RDON by marine bacterioplankton and its subsequent recycling into reduced nitrogen is the sink term that shapes, with ocean transport, the spatial and temporal distribution of RDON. The photoammonification

process is not parameterized but, if so, it would fuel the stock of NH_4 available for phytoplankton and bacterioplankton use, particularly in summer (e.g. Le Fouest et al., 2013; Xie et al., 2013). The RDON contribution to plankton production simulated by the coupled model can thus be considered as a minimum estimate.

From the total input of RDON, only a fraction is directly usable by the plankton (e.g. Wickland et al., 2012). The fraction that enters the coupled model by the 10 river source points is set to 15% of the total RDON input according to a study by Wickland et al. (2012), which suggests that about 15% of the total RDON pool can be degraded within less than one month. This value was chosen based on annual averages calculated from measurements or from model outputs for the Mackenzie River, Yukon River, Kolyma River, Lena River, Yenisey River, and Ob' River (e.g. Wickland et al., 2012). Note, however, that the average values given in Wickland et al. (2012) vary among seasons and rivers. They are the lowest in the Lena River (8%) and the highest in the Ob' River (19%). Maximum values as high as 24% of usable RDON are reported for the Ob' River. Sensitivity analyses with different parameterizations of the usable RDON fraction set amongst river and seasons would hence be informative on the amplitude of the PP and BP response to spatial and temporal variations of the usable RDON flux. To be robust, they should be combined with sensitivity analyses on the freshwater discharge to better constrain the RDON flux. In the Mackenzie River, strong interannual variations in terms of peak of discharge and maximum spring flow were observed in the last four decades (Yang et al., in press). Nevertheless, the use a constant fraction of usable RDON as preformed in the present study provides a first order estimation of its contribution to BP and PP that is consistent with the current state of knowledge about the RDON inputs. In addition to the usable RDON flux into coastal ocean, autochthonous sources of DONl are important in fueling BP. Despite improved BP

323 estimates simulated in the RIV run, the rates remain within the lower range of the observations.
324 It can result from unresolved sources of DONl within the model such as ice-edge and under ice
325 phytoplankton blooms (Arrigo et al., 2012; Perrette et al., 2011), and from missing biological
326 processes like sloppy mesozooplankton feeding and viral lysis.

327 In the biogeochemical model, the usable RDON, dDON, and NH4 produced by the plankton
328 components are taken up by bacterioplankton to build up biomass. The synthesis of cell proteins
329 requires at least carbon and nitrogen. Bacterioplankton obtain all their carbon and some of their
330 nitrogen from DONl (usable RDON + dDON). The simulated NH4 uptake supplements their
331 nitrogen requirements. The growth function is formulated using the Fasham et al. (1990) model.
332 It assumes that in a balanced growth situation, where N and C assimilation occurs
333 simultaneously and where bacterioplankton have fixed stoichiometry, the ratio of NH4 uptake to
334 DONl uptake is constant (0.6, see Appendix A) to ensure that biomass of the required C:N ratio
335 is produced from DONl with a given C:N ratio. If there is not enough NH4 available, the uptake
336 rate of both DONl and NH4 decreases allowing both N and energy limitation. In Arctic waters,
337 the inhibition of DOC uptake by bacterioplankton under inorganic nitrogen limitation was shown
338 by Thingstad et al. (2008). However, as DONl in the model is made a proxy of DOC, the C:N
339 ratio of the substrate is assumed constant. As a consequence, any explicit stoichiometric
340 treatment of the simulated bacterioplankton metabolism is precluded as well as any
341 stoichiometric coupling between DOC and inorganic nutrients (e.g. Thingstad et al., 2008). In
342 addition, the implicit treatment of DOC in the model implies that all of the DOC required for
343 growth is in N-containing forms. Hence it assumes that bacterioplankton cannot be N-limited in
344 substrate. However, N-limitation of bacterioplankton production was observed in summer in
345 surface waters of the Beaufort Sea (Ortega-Retuerta et al., 2012b). This pattern contrasts with the

346 organic carbon limitation observed in the Yenisei and Mackenzie River plumes and adjacent
347 Kara and Beaufort Seas (Meon and Amon, 2004; Vallières et al., 2008), hence highlighting the
348 difficulty to draw a general pattern at the AO scale. Nevertheless, making the C:N ratio of
349 substrates of terrigeneous and marine origin vary in a realistic way in biogeochemical models
350 would farther be required. Single explicit pools of DOC and DON represented as two different
351 state variables, as well as a distinction between readily usable molecules (turnover within days)
352 and more complex ones (turnover within a month) would also make the model more realistic.
353 The parameterization of variable C:N ratios is not trivial as it requires large in-situ datasets (see
354 Letscher et al., 2014) and, in Arctic river-influenced shelf seas, a good knowledge on the
355 characteristics of the terrigenous dissolved organic matter flowing into the coastal ocean (e.g.
356 Mann et al., 2012). Appropriate values for the maximum uptake rates and half-saturation
357 constants may not be easily obtained from existing data in the Arctic. As a result, the coupled
358 model that is used in the present study is an interesting compromise relative to more complex (in
359 terms of number of biological equations and parameters) models of bacterioplankton growth
360 applied to shelf waters (e.g. Auger et al., 2011; Anderson and Williams, 1998).

361 In the model, bacterioplankton compete with phytoplankton for the NH_4 remineralized from the
362 usable RDON and dDON pools. This competition for nutrient resource acts as a bottom-up
363 control of the simulated phytoplankton and bacterioplankton production and, finally, of the
364 BP:PP ratio. For bacterioplankton, the maximum growth rate is temperature normalized. At
365 10°C, which corresponds to a sea surface temperature within the upper range of observations
366 over the shelves in summer, it takes a value of 3 d^{-1}. Hence the NH_4 uptake efficiency (α =
367 maximum growth rate / half-saturation constant for uptake) can reach 30 m^3 mmol N^{-1} d^{-1}, which
368 is about two times higher than for small phytoplankton (14 m^3 mmol N^{-1} d^{-1}). In their study,

Lignell et al. (2013) report values of α that are about 10 times higher for bacterioplankton than for small phytoplankton, hence a larger difference compared to the model. Nevertheless, the difference in α in the model is comparable to that estimated for Isefjord at the entrance of the Baltic Sea (see Lignell et al., 2013). Although the model parameterization can be improved to that respect, the model is in fair agreement with the theoretical and empirical results showing that smaller cells are more efficient in nutrient uptake than larger ones (Lignell et al., 2013). In contrast to bacterioplankton, phytoplankton uptake of inorganic nutrients is also limited by light. In the model, the diffuse attenuation of the incident light caused by the pool of coloured dissolved organic matter (0.05 m^{-1}) is set as constant in the model. This results in the light attenuation in the water column being the same in river plumes as in open and clearer waters. However, river plumes transfer to the coastal marine environment large amounts of optically-active coloured dissolved organic matter of terrigenous origin that strongly attenuate the incident light propagation with depth. As the model does not account for the stronger light attenuation in river plumes, it may overestimate the simulated phytoplankton growth on NH_4 recycled from RDON by bacterioplankton and underestimate the BP in river plumes. As a consequence, the spatial and temporal evolution of the simulated BP:PP ratio can be impacted on shelves. In addition, the ability of Arctic phytoplankton to assimilate low molecular weight DON compounds (50% of total nitrogen assimilated annually; see Simpson et al., 2013) is likely to also play an important role in the phytoplankton-bacterioplankton competition on shelves. A more accurate representation of the simulated underwater light field and uptake of nutrients in river plumes in the coupled model will certainly improve its ability to simulate the competition for nutrients between phytoplankton and bacterioplankton, and hence, predict the temporal evolution of the BP:PP ratio within Arctic waters.

5. Conclusions

A pan-Arctic physical-biogeochemical model was used to quantify the contribution of usable dissolved organic nitrogen drained by the major pan-Arctic rivers on marine bacterioplankton and phytoplankton production in a scenario of melting sea ice (1998-2011). By accounting for the removal of RDON by bacterioplankton in the coupled model, the ability to predict PP and BP in river-influenced shelves is improved. The key points of the study are:

1. On average between 1998 and 2011, the removal of usable RDON by bacterioplankton is responsible for an increase of ~26% in the annual BP, and an increase of ~8% in the total annual PP;
2. Recycled ammonium is responsible for the total PP increase; total summertime PP is increased by ~18%, in average, over 1998-2011;
3. The processing of usable RDON by bacterioplankton promotes a higher annual BP and PP but there is no significant temporal trend in the BP:PP ratio over 1998-2011 on the ice-free shelves; this suggests no significant evolution in the balance between autotrophy and heterotrophy in the last decade with a constant annual flux of RDON into the coastal ocean.

The effect of the predicted warming on the Arctic watersheds is linked to a potential regional increase of RDON inputs into the AO shelf by 32–53 % before the end of the century (Frey and al., 2007). Combined with the accelerated sea ice decline (Comiso et al., 2008) and an increase in seawater temperature on Arctic shelves (Timmermans et al., 2014), this new biogeochemical and physical setting might exacerbate the competing effect for resources

between autotrophs and heterotrophs as sea ice recedes in summer. As a consequence, the metabolic state of the AO shelves could be altered. Nevertheless, to obtain robust predictions of the response of the microbial food web functioning and mass fluxes, coupled models would require improvements in parameterized land-ocean fluxes in terms of spatial and temporal variability of freshwater discharge and nutrients fluxes. In their study combining in-situ datasets and modeling, Holmes et al. (2011) show that annual fluxes of RDOC in the Lena River, estimated between 1999 and 2008, can vary by about a factor of 2. Such variations accentuate the significance of considering the short-term and inter-annual variability of the continental fluxes into the coastal ocean when deriving temporal trends in plankton production and investigating potential changes in trends related to the Arctic warming. Finally, model predictions of future trajectories of PP (e.g. Vancoppenolle et al., 2013) would probably benefit from considering riverine nutrient fluxes as important drivers of PP on Arctic shelves in future decades. However, models that are mechanistically more robust and allow for flexible stoichiometry and N-limitation of bacterial substrate uptake are probably needed for forecasting AO ecosystem responses to climate change scenarios.

Acknowledgments

VLF acknowledges support from the European Space Agency and the Centre national d'études spatiales (CNES) as part of the MALINA project, funded by the Institut national des sciences de l'univers – Centre national de la recherche scientifique (CYBER/LEFE and PICS programmes), the Agence nationale de la recherche and the CNES. MB is supported by the Canada Excellence Research Chair in "Remote sensing of Canada's new Arctic frontier". The authors wish to thank Oliver Jahn from MIT for having kindly provided MITgcm biogeochemical boundary data. We also thank Debra Christiansen-Stowe for English proofreading.

438 **References**

439 Adcroft, A., C. Hill, and J. Marshall (1997), Representation of topography by shaved cells in a
440 height coordinate ocean model, Mon. Weather Rev., 125(9), 2293–2315.

441 Anderson, T. R, and P. J. L. Williams (1998), Modelling the seasonal cycle of dissolved organic
442 carbon at Station E1 in the English Channel, Estuar. Coast. Shelf Sci., 46, 93–109.

443 Arakawa, A., and V. Lamb (1977), Computational design of the basic dynamical processes of the
444 UCLA general circulation model, Methods Comput. Phys., 17, 174–267.

445 Arctic Climate Impact Assessment (2005), Arctic Climate Impact Assessment, 1042 p.,
446 Cambridge Press Univ., New York.

447 Ardyna, M., M. Babin, M. Gosselin, E. Devred, L. Rainville, and J.-E. Tremblay, (2014), Recent
448 Arctic Ocean sea ice loss triggers novel fall phytoplankton blooms, Geophys. Res. Lett., 41,
449 6207-6212, doi:10.1002/2014GL061047.

450 Arrigo, K. R., and G. L. van Dijken (2011), Secular trends in Arctic Ocean net primary
451 production, J. Geophys. Res., 116, C09011.

452 Arrigo, K. R., Perovich, D. K., Pickart, R. S., Brown, Z. W., van Dijken, G. L., Lowry, K. E.,
453 Mills, M. M., Palmer, M. A., Balch, W. M., Bahr, F., Bates, N. R., Benitez-Nelson, C.,
454 Bowler, B., Brownlee, E., Ehn, J. K., Frey, K. E., Garley, R., Laney, S. R., Lubelczyk, L.,
455 Mathis, J., Matsuoka, A., Mitchell, B. G., Moore, G. W., Ortega-Retuerta, E., Pal, S.,
456 Polashenski, C. M., Reynolds, R. A., Schieber, B., Sosik, H. M., Stephens, M., Swift, J. H.
457 (2012), Massive phytoplankton blooms under Arctic sea ice, Science, 336, 1408,
458 doi:10.1126/science.1215065.

459 Auger, P. A., F. Diaz, C. Ulses, C. Estournel, J. Neveux, F. Joux, M. Pujo-Pay, and J. J. Naudin
460 (2011), Functioning of the planktonic ecosystem on the Gulf of Lions shelf (NW
461 Mediterranean) during spring and its impact on the carbon deposition: a field data and 3-D
462 modelling combined approach, Biogeosci., 8, 3231–3261, doi:10.5194/bg-8-3231-2011.

463 Bélanger S., M. Babin, and J.-E.Tremblay (2013), Increasing cloudiness in Arctic damps the
464 increase in phytoplankton primary production due to sea ice receding, Biogeosci., 10, 4087–
465 4101, doi:10.5194/bg-10-4087-2013.

466 Bendsten, J., Lundsgaard, C., Middelboe, M., and D. Archer (2002), Influence of bacterial
467 uptake on deep-ocean dissolved organic carbon, Global Biogeochem. Cycles, 16, 1127,
468 doi:10.1029/2002GB001947.

469 Berline L., Spitz, Y. H., Ashjian, C. J., Campbell, R. G., Maslowski, W., and S. E. Moore (2008),
470 Euphausiid transport in the Western Arctic Ocean, Mar. Ecol. Progr. Ser., 360, 163-178.

471 Bienfang, P., Szyper, J., and E. Laws (1983) Sinking rate and pigment responses to light
472 limitation of a marine diatom: implications to dynamics of chlorophyll maximum layers,
473 Oceanologica Acta 6, 55–62.

474 Bendtsen, J., Lundsgaard, C., Middelboe, M., and D. Archer (2002), Influence of bacterial
475 uptake on deep-ocean dissolved organic carbon, Global Biogeochem. Cycles, 16, 1127,
476 doi:10.1029/2002GB001947.

477 Campbell, R. G., Sherr, E. B., Ashjian, C. J., Plourde. S., Sherr, B. F., Hill, V., and D. A.
478 Stockwell (2009) Mesozooplankton prey preference and grazing impact in the western Arctic
479 Ocean, Deep-Sea Res. (II), 56, 1274–1289, doi: 10.1016/j.dsr2.2008.10.027.

480 Charria, G., Dadou, I., Llido, J., Drévillon, M., and V. Garçon (2008), Importance of dissolved
481 organic nitrogen in the north Atlantic Ocean in sustaining primary production: a 3-D
482 modelling approach, Biogeosci., 5, 1437–1455,

483 Cloern, J. E., Grenz, C., and L. Videgar-Lucas (1995), An empirical model of the phytoplankton
484 chlorophyll:carbon ratio—the conversion factor between productivity and growth rate,
485 Limnol. Oceanogr., 40, 1313–1321.

486 Codispoti, L. A., V. Kelly, A. Thessen, P. Matrai, V. Hill, M. Steele, and B. Light (2013),
487 Synthesis of primary production in the Arctic Ocean: III. Nitrate and phosphate based
488 estimates of net community production, Prog. Oceanogr., 110, 126–150,
489 doi:10.1016/j.ocean.2012.11.006.

490 Condron, A., P. Winsor, C. N. Hill, and D. Menemenlis (2009), Response of Arctic freshwater
491 budget to extreme NAO forcing, J. Clim., 22, 2422–2437.

492 Comiso, J. C., C. L. Parkinson, R. Gersten, and L. Stock (2008), Accelerated decline in the
493 Arctic sea ice cover, Geophys. Res. Lett., 35, L01703, doi:10.1029/2007GL031972.

494 Coupel, P., Jin, H. Y., Joo, M., Horner, R., Bouvet, H. A., Sicre, M.- A., Gascard, J.-C., Chen, J.
495 F., Garçon, V., and D. Ruiz-Pino (2012), Phytoplankton distribution in unusually low sea ice
496 cover over the Pacific Arctic, Biogeosciences, 9, 4835-4850.

497 Dorch, Q. (1990), The interaction between ammonium and nitrate uptake in phytoplankton, Mar.
498 Ecol. Prog. Ser., 61, 183–201.

499 Ducklow, H. W. (1999), The bacterial component of the oceanic euphotic zone, FEMS
500 Microbiology Ecology, 30, 1–10.

501 DuRand, M. D., Green, R. E., Sosik, H. M., and R. J. Olson (2002), Diel variations in Optical
502 properties of Micromonas pusilla (Prasinophyceae), J. Phycol., 38, 1132–1142.

503 Edwards, A. M., and M. A. Bees (2001), Generic dynamics of a simple plankton population
504 model with a non-integer exponent of closure, Chaos Solitons Fractals, 12, 289– 300.

505 Eiane, K., Aksnes, D. L., Ohman, M. D., Wood, S., and M. B. Martinussen (2002), Stage-
506 specific mortality of Calanus spp. under different predation regimes, Limnol. Oceanogr., 47,
507 636– 645.

508 Fasham, M. J. R., Ducklow, H. W., and S. M. McKelvie (1990), A nitrogen-based model of
509 plankton dynamics in the oceanic mixed layer, J. Mar. Res., 48, 591–639.

510 Forest, A., Stemmann, L., Picheral, M., Burdorf, L., Robert, D., Fortier, L., and M. Babin (2012),
511 Size distribution of particles and zooplankton across the shelf-basin system in southeast
512 Beaufort Sea: combined results from an Underwater Vision Profiler and vertical net tows,
513 Biogeosciences, 9, 1301–1320, doi:10.5194/bg-9-1301-2012.

514 Fouilland, E., Gosselin, M., Rivkin, R. B., Vasseur, C., and B. Mostajir (2007), Nitrogen uptake
515 by heterotrophic bacteria and phytoplankton in Arctic surface waters, J. Plankton Res., 29,
516 369-376.

517 Frey, K. E, J. W. McClelland, R. M. Holmes, and L. C. Smith (2007), Impacts of climate
518 warming and permafrost thaw on the riverine transport of nitrogen and phosphorus to the
519 Kara Sea, J. Geophys. Res.-Biogeosciences, 112, G04S58, doi:10.1029/2006JG000369.

520 Garneau, M. E., S. Roy, C. Lovejoy, Y. Gratton, and W. F. Vincent (2008), Seasonal dynamics
521 of bacterial biomass and production in a coastal arctic ecosystem: Franklin Bay, western
522 Canadian Arctic, J. Geophys. Res, 113, C07S91, doi:10.1029/2007JC004281.

523 Geider, R. J., MacIntyre, H. L., and T. M. Kana (1997), Dynamic model of phytoplankton
524 growth and acclimation: responses of the balanced growth rate and the chlorophyll a: carbon
525 ratio to light, nutrient-limitation and temperature. Mar. Ecol. Progr. Ser., 148, 187–200.

526 Guerrero, M. A., and R.D. Jones (1996), Photoinhibition of marine nitrifying bacteria, II. Dark
527 recovery after monochromatic or polychromatic irradiation, Mar. Ecol. Prog. Ser., 141, 193–
528 198

529 Grossart, H.-P., and H. Ploug (2001), Microbial degradation of organic carbon and nitrogen on
530 diatom aggregates, Limnol. Oceanogr., 46, 267– 277.

531 Guidi, L., Jackson, G. A., Stemmann, L., Miquel, J. C., Picheral, M., and G. Gorsky (2008),
532 Relationship between particle size distribution and flux in the mesopelagic zone, Deep-Sea
533 Res. I, 55, 1364-1374.

534 Hibler, W. D., III (1979), A dynamic thermodynamic sea ice model, J. Phys. Oceanogr., 9, 815–
535 846.

536 Hibler, W. D., III, and K. Bryan (1987), A diagnostic ice-ocean model, J. Phys. Oceanogr.,
537 17(7), 987–1015.

538 Hill, V. J., P. Matrai, E. Olson, S. Suttle, M. Steele, L. Codispoti, and R. Zimmerman (2013),
539 Synthesis of integrated primary production in the Arctic Ocean: II. In situ and remotely
540 sensed estimates, Progr. Oceanogr., 110, 107–125, doi:10.1016/j.pocean.2012.11.005.

Holmes, R. M., McClelland, J. W., Peterson, B. J., Tank, S. E., Bulygina, E., Eglinton, T. I., Gordeev, V. V., Gurtovaya, T. Y., Raymond, P. A., Repeta, D. J., Staples, R., Stiegl, R. G., Zhulidov, A. V., and S. A. Zimov (2011), Seasonal and annual fluxes of nutrients and organic matter from large rivers to the Arctic Ocean and surrounding seas, Estuar. Coast, 35, 369–382, doi:10.1007/s12237-011-9386-6.

Jakobsson, M., R. Macnab, L. Mayer, R. Anderson, M. Edwards, J. Hatzky, H. W. Schenke, and P. Johnson (2008), An improved bathymetric portrayal of the Arctic Ocean: Implications for ocean modeling and geological, geophysical and oceanographic analyses, Geophys. Res. Lett., 35, L07602, doi:10.1029/2008GL033520.

Kahru, M., V. Brotas, M. Manzano-Sarabia, and B. G. Mitchell (2011), Are phytoplankton blooms occurring earlier in the Arctic? Global Change Biol., 17, 1733–1739, doi: 10.1111/j.1365-2486.2010.02312.x.

Köhler, H., Meon, B., Gordeev, V. V., Spitzy, A. and R. M. W. Amon (2003) Dissolved organic matter (DOM) in the estuaries of Ob and Yenisei and the adjacent Kara Sea, Russia. In: Stein, R., Fahl, K., Fütterer, D. K., Galimov, E. M., and O. V. Stepanets (Eds.), Siberian River Run-off in the Kara Sea: Characterisation, Quantification, Variability, and Environmental Significance, Proceedings in Marine Sciences, 6, Elsevier, Amsterdam, 281–308.

Kirchman, D. L., and P. A. Wheeler (1998), Uptake of ammonium and nitrate by heterotrophic bacteria and phytoplankton in the sub-Arctic Pacific, Deep-Sea Res. I, 45, 347-365.

Kirchman, D. L., Malmstrom, R. R., and M. T. Cottrell (2005), Control of bacterial growth by temperature and organic matter in the Western Arctic, Deep-Sea Res. II, 52, 3386–3395, doi:10.1016/j.dsr2.2005.09.005.

Kirchman, D. L., Hill, V., Cottrell, M. T., Gradinger, R., Malmstrom, R. R., and A. Parker (2009), Standing stocks, production, and respiration of phytoplankton and heterotrophic bacteria in the western Arctic Ocean, Deep-Sea Res. Pt. II, 56, 1237–1248, doi:10.1016/j.dsr2.2008.10.018.

Kristiansen, S., T. Fabrot, and P. A. Wheeler (1994), Nitrogen cycling in the Barents Sea-Seasonal dynamics of new and regenerated production in the Marginal Ice Zone, Limnol. Oceanogr., 39, 1630–1642.

Lammers, R. B., A. I. Shiklomanov, C. J. Vörösmarty, B. M. Fekete, and B. J. Peterson (2001), Assessment of contemporary Arctic river runoff based on observational discharge records, J. Geophys. Res., 106(D4), 3321–3334.

Lancelot, C., Becquevort, S., Menon, P., Mathot, S., and J.-M. Dandois (1997), Ecological modelling of the planktonic microbial food-web, in Belgian Research Program on the Antarctic, Scientific Results of Phase III (1992 – 1996): Marine Biogeochemistry and Ecodynamics, vol. 1, edited by S. Caschetto, pp. 1–78, Fed. Off. for Sci., Tech. and Cult. Affairs, Brussels.

578 Le Fouest V., B. Zakardjian, F. J. Saucier, and M. Starr (2005), Seasonal versus synoptic
579 variability in planktonic production in a high-latitude marginal sea: the Gulf of St. Lawrence
580 (Canada), J. Geophys. Res., 110, C099012, doi:10.1029/2004JC002423.

581 Le Fouest V., B. Zakardjian, F. J. Saucier, and S. A. Cizmeli (2006), Application of SeaWIFS-
582 and AVHRR-derived data for mesoscale and regional validation of a 3-D high-resolution
583 physical-biological model of the Gulf of St. Lawrence (Canada), 2006. J. Mar. Syst., 60, 30–
584 50.

585 Le Fouest V., C. Postlethwaite, M. A. Morales Maqueda, S. Bélanger, and M. Babin (2011), On
586 the role of tides and strong wind events in promoting summer primary production in the
587 Barents Sea, Cont. Shelf Sci., 31, 1869–1879, doi:10.1016/j.csr.2011.08.013.

588 Le Fouest V., M. Babin, and J.-E . Tremblay (2013a), The fate of riverine nutrients on Arctic
589 shelves, Biogeosci., 10, 3661–3677, doi:10.5194/bg-10-3661-2013.

590 Le Fouest, V., B. Zakardjian, H. Xie, P. Raimbault, F. Joux, and M. Babin (2013b), Modeling
591 plankton ecosystem functioning and nitrogen fluxes in the oligotrophic waters of the Beaufort
592 Sea, Arctic Ocean: a focus on light-driven processes, Biogeosci., 9, 4785–4800,
593 doi:10.5194/bg-10-4785-2013.

594 Lehrter, J. C., Pennock, J. R., and G. B. McManus (1999), Microzooplankton grazing and
595 nitrogen excretion across a surface estuarine-coastal interface, Estuaries, 22, 113– 125.

596 Letscher, R. T., J. K. Moore, Y.-C. Teng, and F. Primeau (2014), Variable C : N : P
597 stoichiometry of dissolved organic matter cycling in the Community Earth System Model,
598 Biogeosciences Discuss., 11, 9071-9101, doi:10.5194/bgd-11-9071-2014.

599 Li, W. K. W., McLaughlin, F. A., Lovejoy, C., and E. C. Carmack (2009), Smallest algae thrive
600 as the Arctic Ocean freshens, Science, 326, 539, doi: 10.1126/science.1179798.

601 Lignell, R., H. Haario, M. Laine, and T. F. Thingstad (2013), Getting the ‘‘right’’ parameter
602 values for models of the pelagic microbial food web, Limnol. Oceanogr., 58, 301–313.

603 Lipschultz, F. (1995), Nitrogen-specific uptake rates of marine phytoplankton isolated from
604 natural populations of particles by flow cytometry, Mar. Ecol. Prog. Ser., 123, 245-258.

605 Manizza, M., M. J. Follows, S. Dutkiewicz, J. W. McClelland, D. Menemenlis, C. N. Hill, A.
606 Townsend-Small, and B. J. Peterson (2009), Modeling transport and fate of riverine dissolved
607 organic carbon in the Arctic Ocean, Global Biogeochem. Cycles, 23, GB4006,
608 doi:10.1029/2008GB003396.

609 Manizza, M., M. J. Follows, S. Dutkiewicz, D. Menemenlis, C. N. Hill, and R. M. Key (2013),
610 Changes in the Arctic Ocean CO2 sink (1996–2007): a regional model analysis, Global
611 Biogeochem. Cycles, 27, 1108–1118, doi: 10.1002/2012GB004491.

612 Mann, P. J., A. Davydova, N. Zimov, R. G. M. Spencer, S. Davydov, E. Bulygina, S. Zimov, and
613 R. M. Holmes (2012), DOM composition and lability during the Arctic spring freshet on the
614 River Kolyma, Northeast Siberia, J. Geophys. Res., 117, G01028,
615 doi:10.1029/2011JG001798.

616 Marshall, J., C. Hill, L. Perelman, and A. Adcroft (1997), Hydrostatic, quasi-hydrostatic and
617 nonhydrostatic ocean modeling, J. Geophys. Res., 102(C3), 5733–5752.

618 McClelland, J. W., et al. (2008), Development of a pan-Arctic database for river chemistry, Eos
619 Trans. AGU, 89(24), 217, doi:10.1029/2008EO240001.

620 MacIntyre, H. L., T. M. Kana, T. Anning, and R. J. Geider (2002), Photoacclimation of
621 photosynthesis irradiance response curves and photosynthetic pigments in microalgae and
622 cyanobacteria, J. Phycology, 38, 17–38.

623 Menemenlis, D., et al. (2005), NASA supercomputer improves prospects for ocean climate
624 research, Eos Trans. AGU, 86(9), 89–96.

625 Meon, B., and R. M. W. Amon (2004), Heterotrophic bacterial activity and fluxes of dissolved
626 free amino acids and glucose in the Arctic rivers Ob, Yenisei and the adjacent Kara Sea,
627 Aquat. Microb. Ecol., 37, 121–135.

628 Morel, A. (1988), Optical modeling of the upper ocean in relation to its biogenous matter content
629 (case I waters). J. Geophys. Res., 93, 10749–10768.

630 National Oceanographic Data Centre World Ocean Atlas 2005 (2006), Documentation
631 accompanying WOA05 DVD (ASCII text and portable document format), Prepared by the
632 Ocean Climate Laboratory, National Oceanographic Data Center, Silver Springs, MD 20910,
633 12 pp.

634 Nedwell, D. B., and M. Rutter (1994), Influence of temperature on growth rate and competition
635 between two psychrotolerant antarctic bacteria: low temperature diminishes affinity for
636 substrate uptake, Applied and Environmental Microbiology, 60, 1984–1992.

637 Ohman, M. D., Eiane, K., Durbin, E. G., Runge, J. A., and H.-J. Hirche (2004), A comparative
638 study of Calanus finmarchicus mortality patterns at five localities in the North Atlantic, ICES
639 J. Mar. Sci., 61, 687–697.

640 Olson, R. J. (1981a), Differential photoinhibition of marine nitrifying bacteria: a possible
641 mechanism for the formation of the primary nitrite maximum, J. Mar. Res., 39, 227–238.

642 Olson, R. J. (1981b), 15N tracers studies of the primary nitrite maximum, J. Mar. Res., 39, 203–
643 226.

644 O'Neill, R. V., DeAngelis, D. L., Pastor, J. J., Jackson, B. J. and W. M. Post (1989), Multiple
645 nutrient limitations in ecological models, Ecol. Model., 46, 147– 163.

646 Onogi, K., J. Tsutsui, H. Koide, M. Sakamoto, S. Kobayashi, H. Hatsushika, T. Matsumoto, N.
647 Yamazaki, H. Kamahori, K. Takahashi, S. Kadokura, K. Wada, K. Kato, R. Oyama, T. Ose,
648 N. Mannoji, and R. Taira (2007), The JRA-25 reanalysis, J. Meteorol. Soc. Jpn., 85(3), 369–
649 432.

650 Opsahl, S., R. Benner, and R. M. W. Amon (1999), Major flux of terrigenous dissolved organic
651 matter through the Arctic Ocean, Limnol. Oceanogr., 44, 2017–2023.

652 Ortega-Retuerta, E., Jeffrey, W. H., Babin, M., Bélanger, S., Benner, R., Marie, D., Matsuoka,
653 A., Raimbault, P., and F. Joux (2012a), Carbon fluxes in the Canadian Arctic: patterns and
654 drivers of bacterial abundance, production and respiration on the Beaufort Sea margin,
655 Biogeosci., 9, 3679–3692.

656 Ortega-Retuerta E., Jeffrey, W. H., Ghiglione, J. F., and F. Joux (2012b), Evidence of
657 heterotrophic prokaryotic activity limitation by nitrogen in the Western Arctic Ocean during
658 summer, Polar Biol., 35, 785-794.

659 Perrette, M., Yool, A., Quartly, G. D., and E. E. Popova (2011), Near-ubiquity of ice-edge
660 blooms in the Arctic, Biogeosci., 8, 515-524, doi:10.5194/bg-8-515-2011.

661 Piontek, J., M. Sperling, E.-M. Nothig, and A. Engel (2014), Regulation of bacterioplankton
662 activity in Fram Strait (Arctic Ocean) during early summer: the role of organic matter supply
663 and temperature, J. Mar. Syst., 132, 83–94.

664 Rachold, V., H. Eiken, V. V. Gordeev, M. N. Grigoriev, H.-W. Hubberten, A. P. Lisitzin, V. P.
665 Shevchenko, and L. Schirmeister (2004), Modern terrigenous organic carbon input to the
666 Arctic Ocean, In: The Organic Carbon Cycle in the Arctic Ocean, edited by R. S. Stein and
667 R. W. Macdonald, 33–55, Springer, New York.

668 Raymond, P. A., J. W. McClelland, R. M. Holmes, A. V. Zhulidov, K. Mull, B. J. Peterson, R.
669 G. Striegl, G. R. Aiken, and T. Y. Gurtovaya (2007), Flux and age of dissolved organic
670 carbon exported to the Arctic Ocean: A carbon isotopic study of the five largest arctic rivers,
671 Global Biogeochem. Cycles, 21, GB4011, doi:10.1029/2007GB002934.

672 Redfield, A. C., B. H., Ketchum, and F. A. Richards (1973), The influence of organisms on the
673 composition of sea water, in The Sea: Ideas and Observations on Progress in the Study of the
674 Seas, edited by M. N. Hill, pp. 26–27, Wiley-Intersci., Hoboken, N. Y.

675 Rich, J., M. Gosselin, E. Sherr, B. Sherr, and D. L. Kirchman (1997), High bacterial production,
676 uptake and concentrations of dissolved organic matter in the Central Arctic Ocean, Deep Sea
677 Res., Part II, 44, 1645– 1663, doi:10.1016/S0967-0645(97)00058-1.

678 Sakshaug, E. (2004), Primary and Secondary Production in the Arctic Seas, In: The Organic
679 Carbon Cycle in the Arctic Ocean (Eds. Stein, R., and R. W. Macdonald), 57–81,
680 10.1007/978-3-642-18912-8_3, Springer Berlin Heidelberg.

681 Sahzin, A. F., N. D. Romanova, and S. A. Mosharov (2010), Bacterial and primary production in
682 the pelagic zone of the Kara Sea, Oceanology, 50, 759–765.

683 Serreze, M., A. P. Barret, A. G. Slater, R. A. Woodgate, K. Aagard, R. B. Lammers, M. Steele,
684 R. Mortitz, M. Meredith, and C. M. Lee (2006), The large-scale fresh water cycle of the
685 Arctic, J. Geophys. Res., 111, C11010, doi:10.1029/2005JC003424.

686 Sherr, E. B., Sherr, B. F., Wheeler, P. A., and K. Thompson (2003), Temporal and spatial
687 variation in stocks of autotrophic and heterotrophic microbes in the upper water column of
688 the central Arctic Ocean, Deep-Sea Res. I, 50, 557–571, doi:10.1016/S0967-0637(03)00031-
689 1.

690 Shiklomanov, I., A. Shiklomanov, R. Lammers, B. Peterson, and C. Vorosmarty (2000), The
691 dynamics of river water inflow to the Arctic Ocean, in The Freshwater Budget of the Arctic
692 Ocean, edited by E. Lewis, pp. 281–296, Kluwer Acad., Dordrecht, Netherlands.

693 Shiklomanov, A. and Lammers, R. B. (2011), River discharge (in Arctic, Report Card 2011),
694 available at http://www.arctic.noaa.gov/report11/river_discharge.html, (last access: 27
695 October, 2014).

696 Sibert, V., Zakardjian, B., Gosselin, M., Starr, M., Senneville, S., LeClainche, Y. 2011. 3D bio-
697 physical model of the sympagic and planktonic productions in the Hudson Bay System. J.
698 Mar. Syst. 88, 401–422, 10.1016/j.jmarsys.2011.03.014.

699 Simpson, K. G., J.-É Tremblay, S. Brugel, and N. M. Price (2013), Nutrient dynamics in the
700 western Canadian Arctic. II. Estimates of new and regenerated production over the
701 Mackenzie Shelf and Cape Bathurst Polynya, Mar. Ecol. Prog. Ser., 484, 47–62, doi:
702 10.3354/meps10298.

703 Steele, J. H., and E. W. Henderson (1992), The role of predation in plankton models, J. Plankton
704 Res., 14, 157– 172.

705 Steele, M., R. Morley, and W. Ermold (2001), PHC: A global ocean hydrography with a high
706 quality Arctic Ocean, J. Clim., 14, 2079–2087, doi:10.1175/1520-0442(2001).

707 Steele, M., W. Ermold, and J. Zhang (2008), Arctic Ocean surface warming trends over the past
708 100 years, Geophys. Res. Letters, 35, L02614, doi:10.1029/2007GL031651.

709 Steward, G. F., D. C. Smith, and F. Azam (1996), Abundance and production of bacteria and
710 viruses in the Bering and Chukchi Seas, Mar. Ecol. Prog. Ser., 131, 287–300.

711 Straile, D. (1997), Gross growth efficiencies of protozoan and metazoan zooplankton and their
712 dependence on food concentration, predator-prey weight ratio, and taxonomic group, Limnol.
713 Oceanogr., 42, 1375-1385.

714 Sturluson M., T. G. Nielsen, and P. Wassmann (2008), Bacteria abundance, biomass and
715 production during spring blooms in the northern Barents Sea, Deep-Sea Res. II, 55, 2186–
716 2198.

717 Taniguchi, A. (1999), Differences in structure of lower trophic levels of pelagic ecosystems in
718 the eastern and western subarctic Pacific, Prog. Oceanogr., 43, 289–315.

719 Tank, S. E., M. Manizza, R. M. Holmes, J. W. McClelland, and B. J. Peterson (2012), The
720 processing and impact of dissolved riverine nitrogen in the Arctic Ocean, Estuar. Coasts, 35,
721 401–415, doi:10.1007/s12237-011-9417-3.

722 Thingstad, F. T, R. G. J. Bellerby, G. Bratbak, K. Y. Børsheim, J. K. Egge, M. Heldal, A.
723 Larsen, C. Neill, J. Nejstgaard, S. Norland, R.-A. Sandaa, E. Skjoldal, T. Tanaka T, R.
724 Thyrhaug, and B. Töpper (2008), Counterintuitive carbon-to-nutrient coupling in an Arctic
725 pelagic ecosystem, Nature, 455, 387–390.

726 Timmermans, M.-L., and 21 others (2014), Arctic Ocean Sea Surface Temperature (in Arctic
727 Report Card), available at
728 http://www.arctic.noaa.gov/reportcard/ocean_temperature_salinity.html, (last access: 27
729 October, 2014).

730 Tremblay, J.-É., Legendre, L., Klein, B. and J.-C. Therriault (2000), Size differential uptake of
731 nitrogen and carbon in a marginal sea (Gulf of St. Lawrence, Canada): Significance of diel
732 periodicity and urea uptake, Deep Sea Res., Part II, 47, 489–518.

733 Vancoppenolle, M., L. Bopp, G. Madec, J. Dunne,T. Ilyina, P. R. Halloran, and N. Steiner
734 (2013), Future Arctic Ocean primary productivity from CMIP5 simulations: Uncertain
735 outcome, but consistent mechanisms, Global Biogeochem. Cycles, 27, 605–619, doi:
736 10.1002/gbc.20055.

737 Vallières C., L. Retamal, C. Osburn, and W. F. Vincent (2008), Bacterial production and
738 microbial food web structure in a large Arctic river and the coastal Arctic Ocean, J. Mar.
739 Syst., 74:756–773, doi: 10.1016/j.jmarsys.2007.12.002.

740 Wickland, K. P., G. R. Aiken, K. Butler, M. M. Dornblaser, R. G. M. Spencer, and R. G. Striegl
741 (2012), Biodegradability of dissolved organic carbon in the Yukon River and its tributaries:
742 Seasonality and importance of inorganic nitrogen, Global Biogeochem. Cycles, 26, GB0E03,
743 doi:10.1029/2012GB004342.

744 Xie, H., Bélanger, S., Song, G., Benner, R., Taalba, A., Blais, M., Le Fouest, V., Tremblay, J.-É.,
745 and M. Babin (2012), Photoproduction of ammonium in the Southeastern Beaufort Sea and
746 its biogeochemical implications, Biogeosciences, 9, 3047–3061, doi:10.5194/bg-9-3047-
747 2012.

748 Yang, D., Shic, X., and P. Marsh (in press), Variability and extreme of Mackenzie River daily
749 discharge during 1973–2011, Quaternary International, DOI: 10.1016/j.quaint.2014.09.023.

750 Zhang, J., and W. D. Hibler III (1997), On an efficient numerical method for modeling sea ice
751 dynamics, J. Geophys. Res., 102, 8691–8702.

752 Zhang, J., and D. Rothrock (2003), Modeling global sea ice with a thickness and enthalpy
753 distribution model in generalized curvilinear coordinates, Mon. Weather Rev., 131(5), 845–
754 861, doi:10.1175/1520-0493(2003) 131<0845:MGSIWA>2.0.CO;2.

755

List of tables captions

Table 1. Differential equations for the 10-component biogeochemical model: nitrate (NO_3), ammonium (NH_4), large and small phytoplankton (LP and SP, respectively), large and small zooplankton (LZ and SZ, respectively), bacterioplankton (BACT), detrital particulate and dissolved organic nitrogen (dPON and dDON, respectively), and usable riverine dissolved organic nitrogen (RDON).

Table 2. Biogeochemical model parameters.

765 **List of figures captions**

766 **Figure 1.** Conceptual diagram of the biogeochemical model. The 10 state variables are nitrate
767 (NO_3), ammonium (NH_4), large (>5μm) and small (<5μm) phytoplankton, large zooplankton,
768 protozooplankton, bacterioplankton, detrital particulate and dissolved organic nitrogen (dPON
769 and dDON, respectively), and usable riverine dissolved organic nitrogen (RDON). Green, red
770 and blue arrows represent nutrient uptake, grazing and nitrogen recycling, respectively.

771 **Figure 2.** Mean annual ocean primary production (gC m^{-2}) over 1998-2011 a) without RDON
772 removal by bacterioplankton (CTRL run), b) with RDON removal by bacterioplankton (RIV
773 run), and c) absolute difference (gC m^{-2}; RIV run – CTRL run).

774 **Figure 3.** Mean annual new primary production (gC m^{-2}; upper panels) and NH_4-supported
775 primary production (gC m^{-2}; lower panels) over 1998-2011 simulated in the CTRL run (left
776 panels a and d) and the RIV run (middle panels b and e). Right panels (c and f) provide the
777 absolute difference (gC m^{-2}; RIV run – CTRL run).

778 **Figure 4.** Seasonal climatology of the 0-50 m integrated bacterial biomass (mmolN m^{-2}) for
779 spring (upper panels) and summer (lower panels) over the 1998-2011 period simulated in the
780 CTRL run (left panels a and d) and in the RIV run (middle panels b and e). Right panels (c and f)
781 provide the absolute difference (gC m^{-2}; RIV run – CTRL run).

782 **Figure 5.** Time course of primary production (PP, TgC yr^{-1}) (top panel), bacterioplankton
783 production (BP, TgC yr^{-1}) (middle panel), and of the BP:PP ratio in the ice-free shelves (see text
784 for details) of the Arctic Ocean domain (> 66.5 °N) simulated in the RIV run. The dashed
785 straight lines represent the linear trend computed over the 1998-2011 period.

786

787 **Table 1.**

$$\frac{\partial NO_3}{\partial t} = -\nabla \cdot (\mathbf{u}NO_3 - \mathbf{K} \cdot \nabla NO_3) + nitrif - lim_{NO_3}^{LP}\mu_{LP}LP - lim_{NO_3}^{SP}\mu_{SP}SP$$

$$\frac{\partial NH_4}{\partial t} = -\nabla \cdot (\mathbf{u}NH_4 - \mathbf{K} \cdot \nabla NH_4) - lim_{NH_4}^{LP}\mu_{LP}LP - lim_{NH_4}^{SP}\mu_{SP}SP - nitrif$$
$$- Ubact_{NH_4}(1 - ge_{BACT})BACT + (1 - eg_{SZ})(1 - ge_{SZ})G_{SZ}SZ + ex_{LZ}LZ$$

$$\frac{\partial LP}{\partial t} = -\nabla \cdot (\mathbf{u}LP - \mathbf{K} \cdot \nabla LP) + \mu_{LP}LP - G_{LZ}pf_{LP}LZ - m_{LP}LP + \frac{\partial}{\partial z}\left(sed_{lp}LP\right)$$

$$\frac{\partial SP}{\partial t} = -\nabla \cdot (\mathbf{u}SP - \mathbf{K} \cdot \nabla SP) + \mu_{SP}SP - G_{SZ}pf_{SP}SZ - m_{SP}SP$$

$$\frac{\partial LZ}{\partial t} = -\nabla \cdot (\mathbf{u}LZ - \mathbf{K} \cdot \nabla LZ) + assim_{LZ}G_{LZ}LZ - m_{LZ}LZ^2 - ex_{LZ}LZ$$

$$\frac{\partial SZ}{\partial t} = -\nabla \cdot (\mathbf{u}SZ - \mathbf{K} \cdot \nabla SZ) + ge_{SZ}G_{SZ}SZ - m_{SZ}SZ^2 - G_{LZ}(1 - pf_{LP})LZ$$

$$\frac{\partial BACT}{\partial t} = -\nabla \cdot (\mathbf{u}BACT - \mathbf{K} \cdot \nabla BACT) + Ubact_{NH_4}ge_{BACT}BACT + Ubact_{DONl}ge_{BACT}BACT$$
$$- m_{BACT}BACT - G_{SZ}(1 - pf_{SP})SZ$$

$$\frac{\partial dPON}{\partial t} = -\nabla \cdot (\mathbf{u}dPON - \mathbf{K} \cdot \nabla dPON) + (1 - assim_{LZ})G_{LZ}LZ + m_{LZ}LZ^2 + m_{LP}LP$$
$$+ \frac{\partial}{\partial z}\left(sed_{dpon}dPON\right) - f_g dPON$$

$$\frac{\partial dDON}{\partial t} = -\nabla \cdot (\mathbf{u}dDON - \mathbf{K} \cdot \nabla dDON) + f_g dPON + m_{SZ}SZ^2 + m_{SP}SP + m_{BACT}BACT$$
$$+ (1 - eg_{SZ})(1 - ge_{SZ})G_{SZ}SZ - Ubact_{DONl}pf_{dDON}(1 - ge_{BACT})BACT$$

$$\frac{\partial RDON}{\partial t} = -\nabla \cdot (\mathbf{u}RDON - \mathbf{K} \cdot \nabla RDON) - Ubact_{DONl}(1 - pf_{dDON})(1 - ge_{BACT})BACT$$

788

789

790 **Table 2.**

Symbol	Description	Value	Units
NUTRIENTS			
$nitrif_{max}$	Maximum NH_4 nitrification rate	0.05	d^{-1}
K_{nitrif}^{N}	Half-saturation constant for NH_4 nitrification	0.07	mmol N m^{-3}
PHYTOPLANKTON			
kw	Light attenuation coefficient due to water	0.04	m^{-1}
$knonchl$	Light attenuation coefficient due to nonchlorophyllous matter	0.05	m^{-1}
$K_{NO_3}^{LP}$	Half-saturation constant for NO_3 use by LP	1	mmol N m^{-3}
$K_{NO_3}^{SP}$	Half-saturation constant for NO_3 use by SP	1	mmol N m^{-3}
$K_{NH_4}^{LP}$	Half-saturation constant for NH_4 use by LP	0.5	mmol N m^{-3}
$K_{NH_4}^{SP}$	Half-saturation constant for NH_4 use by SP	0.1	mmol N m^{-3}
K_E^{LP}	Photoacclimation parameter	8	Ein m^{-2} d^{-1}
K_E^{SP}	Photoacclimation parameter	4	Ein m^{-2} d^{-1}
$\left(\frac{Chl}{C}\right)_{max}^{LP}$	Maximum Chl to C ratio for LP	0.0125	g g^{-1}
$\left(\frac{Chl}{C}\right)_{max}^{SP}$	Maximum Chl to C ratio for SP	0.007	g g^{-1}
μ_{max}^{LP}	Maximum growth rate for LP	1.4	d^{-1}
μ_{max}^{SP}	Maximum growth rate for SP	1.4	d^{-1}
α_{SP}	Initial slope of the photosynthesis-irradiance curve	5.5	mg C (mg Chl)$^{-1}$ (Ein m^{-2} d^{-1})$^{-1}$
α_{LP}	Initial slope of the photosynthesis-irradiance curve	7.5	mg C (mg Chl)$^{-1}$ (Ein m^{-2} d^{-1})$^{-1}$
sed_lp	LP sinking rate	2	m d^{-1}
m_{LP}	LP senescence	0.05	d^{-1}
m_{SP}	SP senescence	0.05	d^{-1}
ZOOPLANKTON			
G_{LZ}^{max}	Maximum grazing rate for LZ	0.3	d^{-1}
λ	Ivlev constant for LZ	0.5	(mmol N m^{-3})$^{-1}$
G_{SZ}^{max}	Maximum grazing rate for SZ	1	d^{-1}
K_G	Half-saturation constant for SZ grazing	0.8	mmol N m^{-3}
$assim_{LZ}$	LZ assimilation efficiency	70	%
ge_{SZ}	SZ growth efficiency	30	%
eg_{SZ}	dDON egestion by SZ	40	%
ex_{LZ}	NH_4 excretion by LZ	0.05	d^{-1}
m_{SZ}	SZ mortality	0.05	(mmol N m^{-3})$^{-1}$
m_{LZ}	LZ mortality	0.2	(mmol N m^{-3})$^{-1}$
BACTERIOPLANKTON			
$Ubact_{max}$	Temperature normalized maximum growth rate	1	d^{-1}

$K_{NH_4}^{BACT}$	Half-saturation constant for NH_4 uptake	0.1	mmol N m^{-3}
K_{DONl}^{BACT}	Half-saturation constant for DONl uptake	0.1	mmol N m^{-3}
ge_{BACT}	Growth efficiency	20	%
m_{BACT}	Senescence	0.05	d^{-1}
DETRITUS			
sed_dpon	dPON sinking rate	100	m d^{-1} (mmol N m^{-3})$^{-1}$
f_g	dPON fragmentation rate	0.05	d^{-1}

791

792

Appendix

The set of differential equations that include the mechanistic formulations cited below is given in Table 1. The biological parameters related to the mathematical equations are detailed in Table 2.

Phytoplankton

The growth rate ($\mu^{LP,SP}$, d^{-1}) of large and small phytoplankton (LP and SP, respectively) depends on both light and nitrogen availability. It is computed according to the Liebig's Law of the minimum between the nutrient-based and light-based growth rates ($\mu_N^{LP,SP}$ and $\mu_{light}^{LP,SP}$, respectively):

$$\mu^{LP,SP} = \left(\mu_N^{LP,SP}, \mu_{light}^{LP,SP}\right)_{min} \quad (1)$$

The nutrient-based growth rate is computed as follows:

$$\mu_N^{LP,SP} = \mu_{max}^{LP,SP} lim_N^{LP,SP} \quad (2)$$

where $\mu_{max}^{LP,SP}$ is the maximum growth rate and $lim_N^{LP,SP}$ the total nutrients limitation term (dimensionless) computed according to the substitutable model of O'Neill et al. (1989):

$$lim_N^{LP,SP} = \frac{NO_3 K_{NH_4}^{LP,SP} + NH_4 K_{NO_3}^{LP,SP}}{NO_3 K_{NH_4}^{LP,SP} + NH_4 K_{NO_3}^{LP,SP} + K_{NH_4}^{LP,SP} K_{NO_3}^{LP,SP}} \quad (3)$$

$$lim_{NO_3}^{LP,SP} = \frac{NO_3 K_{NH_4}^{LP,SP}}{NO_3 K_{NH_4}^{LP,SP} + NH_4 K_{NO_3}^{LP,SP}} \quad (4)$$

$$lim_{NH_4}^{LP,SP} = \frac{NH_4 K_{NO_3}^{LP,SP}}{NO_3 K_{NH_4}^{LP,SP} + NH_4 K_{NO_3}^{LP,SP}} \quad (5)$$

where $lim_{NO_3}^{LP,SP}$ and $lim_{NH_4}^{LP,SP}$ are the nitrate (NO_3) and ammonium (NH_4) uptake fractions (dimensionless), respectively. $K_{NH_4}^{LP,SP}$ and $K_{NO_3}^{LP,SP}$ are the half-saturation constants for NH_4 and

808 NO_3 uptake, respectively. NH_4 is set to be the preferred inorganic nitrogen source (Dorch, 1990)
809 with a higher affinity for SP (Tremblay et al., 2000). This is expressed in the model by half-
810 saturation constants for NH_4 uptake ($K_{NH_4}^{LP,SP}$) lower than for NO_3 that, when used with the
811 substitutable model, allow for an inhibitory effect of NH_4 on NO_3 uptake as often observed
812 (Dorch, 1990). It implies that NO_3 uptake by LP and SP is inhibited by NH_4 at concentrations
813 two-fold and ten-fold lower than NO_3 concentrations, respectively. The equation used to
814 compute the light-based growth rate is:

$$\mu_{light}^{LP,SP} = \mu_{max}^{LP,SP} lim_{light}^{LP,SP} \quad (6)$$

815 where $lim_{light}^{LP,SP}$ is the light limitation term (dimensionless) expressed as:

$$lim_{light}^{LP,SP} = 1 - e^{-\frac{E_z}{E_k^{LP,SP}}} \quad (7)$$

816 where $E_k^{LP,SP}$ is the light saturation parameter (Ein m^{-2} d^{-1}) computed as follows:

$$E_k^{LP,SP} = \left(\frac{C}{Chl}\right)^{LP,SP} \frac{\mu_{max}^{LP,SP}}{\alpha_{LP,SP}} \quad (8)$$

817 where C:Chl is the carbon to Chl ratio (g g^{-1}) and $\alpha_{LP,SP}$ is the initial slope (mg C (mg Chl)$^{-1}$ (Ein
818 m^{-2} d^{-1})$^{-1}$) of the photosynthesis-irradiance curve. Photoacclimation translates the adaptative
819 response through varying C:Chl ratios in response to light and nutrient availability (e.g. Cloern et
820 al., 1995; Geider et al., 1997; MacIntyre et al., 2002).

821 Varying C:Chl ratios are computed using a modified version of the empirical relationship of
822 Cloern et al. (1995) successfully applied to Hudson Bay in the Arctic (Sibert et al., 2011). The
823 ratios can vary up to 4- to 6-fold based on the general photoacclimation rule given by MacIntyre
824 et al. (2002) and on Arctic nano- and picophytoplankton data (DuRand et al., 2002; Sherr et al.,
825 2003) as follows:

$$\left(\frac{Chl}{C}\right)^{LP} = \left(\frac{Chl}{C}\right)^{LP}_{max}\left(1 + 4e^{-0.5\frac{E_z}{K_E^{LP}}lim_N^{LP}}\right) \quad (9)$$

$$\left(\frac{Chl}{C}\right)^{SP} = \left(\frac{Chl}{C}\right)^{SP}_{max}\left(1 + 5e^{-0.5\frac{E_z}{K_E^{SP}}lim_N^{SP}}\right) \quad (10)$$

where $K_E^{LP,SP}$ is the half-saturation parameter driving the curvature of the C:Chl versus light relationship. E_z (Ein m^{-2} d^{-1}) is the downwelling PAR propagating within the water column according to the Beer-Lambert Law:

$$E_z = PAR0 \int \mathrm{e}^{-[(kchl+kw+knonchl)z]}\mathrm{dz} \quad (11)$$

where PAR0 is the PAR just below the sea surface. The diffuse attenuation of PAR with depth (z) is due to the simulated Chl ($kchl$) (m^{-1}; Morel, 1988), water molecules (kw) (0.04 m^{-1}; Morel, 1988) and non-chlorophyllous matter ($knonchl$). $knonchl$ is set to 0.05 m^{-1}. $kchl$ is calculated according to Morel et al. (1988) as follows:

$$kchl = 0.0518(Chl)^{-0.572}Chl \quad (12)$$

with

$$Chl = 12\left(\frac{106}{16}\right)\left[LP\left(\frac{Chl}{C}\right)^{LP} + SP\left(\frac{Chl}{C}\right)^{SP}\right] \quad (13)$$

Apart from grazing, phytoplankton loss terms include senescence and sinking for LP. LP sinking rates vary in the model from 0 to 2 m d^{-1} depending on nutrient availability (Bienfang et al., 1983):

$$sed_{lp} = sed\_lp(1 - lim_N^{LP}) \quad (14)$$

where sed_lp is a constant.

Zooplankton

Mathematical formulations and parameters related to large zooplankton (LZ) dynamics were chosen to primarily reflect mesozooplankton. Grazing (G_{LZ}, d^{-1}) is described by an Ivlev function:

$$G_{LZ} = G_{LZ}^{max}\left[\left(1 - e^{-\lambda(LP+SZ)}\right)\right] \quad (15)$$

LZ graze upon LP and protozooplankton (SZ) with a prey-specific grazing rate assumed to be proportional to the relative biomass of the prey (Campbell et al., 2009) defined for LP as follows:

$$pf_{LP} = \frac{LP}{LP + SZ} \quad (16)$$

Losses in LZ biomass are due to NH_4 release, fecal pellet production (non-assimilated nitrogen ingested) and mortality. Mortality encompasses senescence and predation (Eiane et al., 2002). It is described by a density-dependent quadratic function. It implicitly represents cannibalism as well as predation by macrozooplankton (Forest et al., 2012; Berline et al., 2008) and limits the occurrence of oscillations generated in such non-linear systems (Edwards and Bees, 2001). The constant of mortality is set to 0.2 (mmol N m^{-3})$^{-1}$ to simulate realistic mortality rates (e.g. Ohman et al., 2004).

SZ grazing (G_{SZ}) upon SP and bacterioplankton (BACT) is formulated by a sigmoidal "Holling-type-III" function:

$$G_{SZ} = G_{SZ}^{max}\frac{(SP + BACT)^2}{(SP + BACT)^2 + {K_G}^2} \quad (17)$$

where G_{SZ}^{max} and K_G are the maximum grazing rate (d^{-1}) and the half-saturation constant for grazing (mmol N m^{-3}), respectively. The grazing function provides a threshold-like limit for low SP biomass that enhances the biological system stability (e.g. Steele and Henderson, 1992). In polar waters, there is evidence that protozooplankton only exert a control on small phytoplankton biomass beyond a threshold (Lancelot et al., 1997). As for LZ, SZ graze upon both SP and

BACT with a prey-specific grazing rate (d^{-1}) assumed to be proportional to the relative biomass of the prey defined for SP as follows:

$$pf_{SP} = \frac{SP}{SP + BACT} \quad (18)$$

We set the fraction of food ingested and converted into biomass to 30 % (Straile, 1997). Lehrter et al. (1999) report that >30 % of the total nitrogen release by SZ could be in the dissolved organic form. In the model, assuming that 40 % is released as detrital DON (dDON), the 60 % remaining are lost as NH_4. Other SZ loss terms are grazing by LZ and mortality. Similarly to LZ, SZ mortality is expressed by a density-dependent quadratic function to encompass grazing amongst SZ.

Bacterioplankton

Bacterioplankton is explicitly simulated following the model of Fasham et al. (1990). They grow on NH_4, dDON and usable RDON. Usable RDON is considered as 15% of total RDON (e.g. Wickland et al., 2012) and is converted into N currency (RDON) using a C:N ratio of 40 (Tank et al., 2012; Köhler et al., 2003). Dissolved organic matter (DOM) is a complex bacterial substrate representing a source of nitrogen (DON) and carbon (DOC). As nitrogen is the sole currency of the model, the simulated DONl is made a proxy of DOC for bacterioplankton uptake. This means that bacterioplankton in the model obtain all of their carbon and some of their nitrogen from the usable fraction of RDON and from detrital DON (dDON). This assumes that all of the DOC required for growth is in N-containing forms. By contrast, the simulated ammonium uptake supplements the bacterioplankton N requirements for growth. The DONl uptake rate ($Ubact_{DONl}$, d^{-1}) is represented by a Michaelis-Menten model:

$$Ubact_{DONl} = Ubact_{max}\left(\frac{DONl}{K_{DONl}^{BACT} + S + DONl}\right)Q_{10} \quad (19)$$

where K_{DONl}^{BACT} is the half-saturation constant for DONl uptake (mmol N m^{-3}), and S the total nitrogenous substrate (mmol N m^{-3}) defined as:

$$S = (\mathrm{NH_4}, 0.6\mathrm{DONl})_{min} \quad (20)$$

According to the study by Bendtsen et al. (2002) in the Greenland Sea, a Q_{10} function was introduced using a Q_{10}-factor of 3 (Kirchman et al., 2005):

$$Q_{10} = 3^{\frac{T}{10}} \quad (21)$$

where T is the simulated seawater temperature. A temperature normalized maximum uptake rate ($Ubact_{max}$) of 1 d^{-1} was used to simulate maximum growth rates in line with those measured in polar waters (e.g. Nedwell and Rutter, 1994). A growth efficiency of 20% (Ortega-Retuerta et al., 2012; Meon and Amon, 2004) was imposed. The fractionning of the two DONl pools (i.e. usable RDON and dDON) is set as follows:

$$pf_{dDON} = \frac{dDON}{dDON + RDON} \quad (22)$$

Similarly, the uptake rate of NH_4 ($Ubact_{NH_4}$, d^{-1}) is represented as follows:

$$Ubact_{NH_4} = Ubact_{max}\left(\frac{S}{K_{NH_4}^{BACT} + S + DONl}\right)Q_{10} \quad (23)$$

where $K_{NH_4}^{BACT}$ is the half-saturation constant for NH_4 uptake (mmol N m^{-3}). This formulation ensures that the uptake of NH_4 will be 0.6-fold the uptake of DONl, as required by the balanced growth model (e.g. Fasham et al., 1990). BACT cannot grow on NO_3 in the model. NO_3 uptake is an energetically expensive process so that bacterioplankton usually accounts for more ammonium than nitrate uptake (Lipschultz, 1995). Furthermore, although a substantial nitrate uptake by bacterioplankton was reported at high latitudes, it occurred in very specific conditions

897 such as in high nitrate low chlorophyll waters (Kirchman and Wheeler, 1998) or in low
898 chlorophyll waters dominated by cyanobacteria (Fouilland et al., 2007). Such conditions are not
899 achieved in the model. Senescence is in the NH_4 form, and it represents 5% of the biomass.
900
901 *Detritus*
902 The pool of detrital particulate organic nitrogen (dPON) is fueled by the production of fecal
903 pellets by LZ, and by LZ and LP mortality. The sedimentation loss term (d^{-1}) is expressed as a
904 quadratic function allowing for the implicit increasing aggregation of particles with increasing
905 dPON concentration (see Guidi et al., 2008):

$$sed_{pon} = sed\_dpon(dPON) \quad (24)$$

906 where sed_dpon is the sedimentation constant (m d^{-1} (mmol N m^{-3})$^{-1}$). The second loss term is
907 the dPON fragmentation into dDON (e.g. Grossart and Ploug, 2001).
908 The dDON pool results from dPON fragmentation, SP, SZ, and BACT mortality and SZ
909 release. It is explicitly remineralized into NH_4 by BACT.
910
911 *Nutrients*
912 NH_4 resulting from the remineralization by BACT and from the LZ and SZ release fuels
913 regenerated primary production and BACT production. In turn, NH_4 undergoes nitrification (d^{-1})
914 into NO_3 as follows:

$$nitrif = nitrif_{max}\left(\frac{NH_4}{NH_4 + K^N_{nitrif}}\right)\left(1 - \frac{E_z}{E_z + K^{light}_{nitrif}}\right) \quad (25)$$

915 Where $nitrif_{max}$ is the maximum nitrification rate (d^{-1}), and K_{nitrif}^{N} and K_{nitrif}^{light} the half-
916 saturation constants for NH_4 (mmol N m^{-3}) and light (Ein m^{-2} d^{-1}) use, respectively. The latter is
917 defined as a fraction of surface PAR (E_0) as follows:

$$K_{nitrif}^{light} = 0.005E_0 \quad (26)$$

918 Mean values taken from the literature (Guerrero and Jones, 1996; Olson, 1981ab) are used to set
919 parameters.

920

921

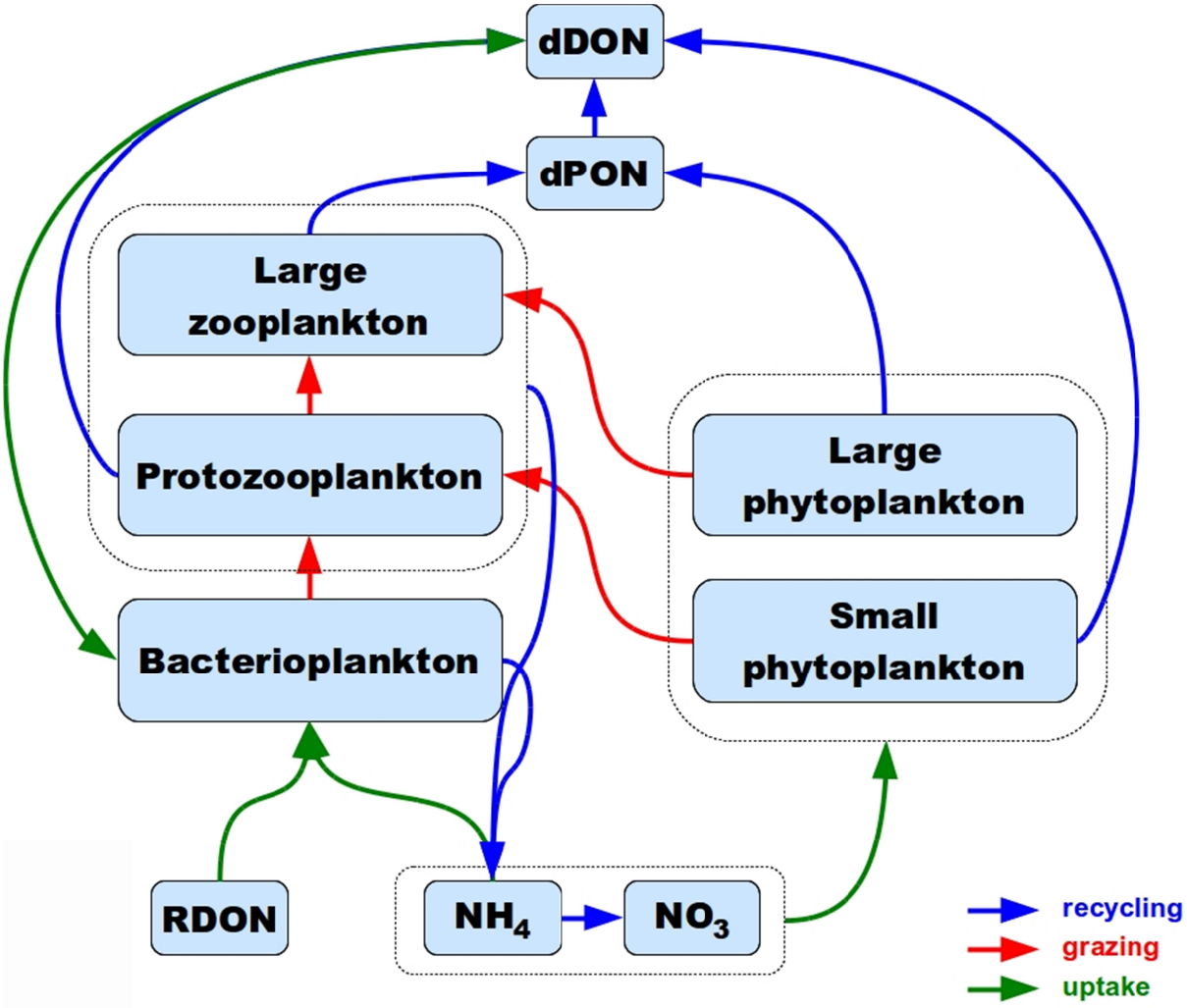
dDON
dPON
Large zooplankton
Protozooplankton
Bacterioplankton
Large phytoplankton
Small phytoplankton
RDON
NH_4
NO_3
recycling
grazing
uptake

Figure 1.

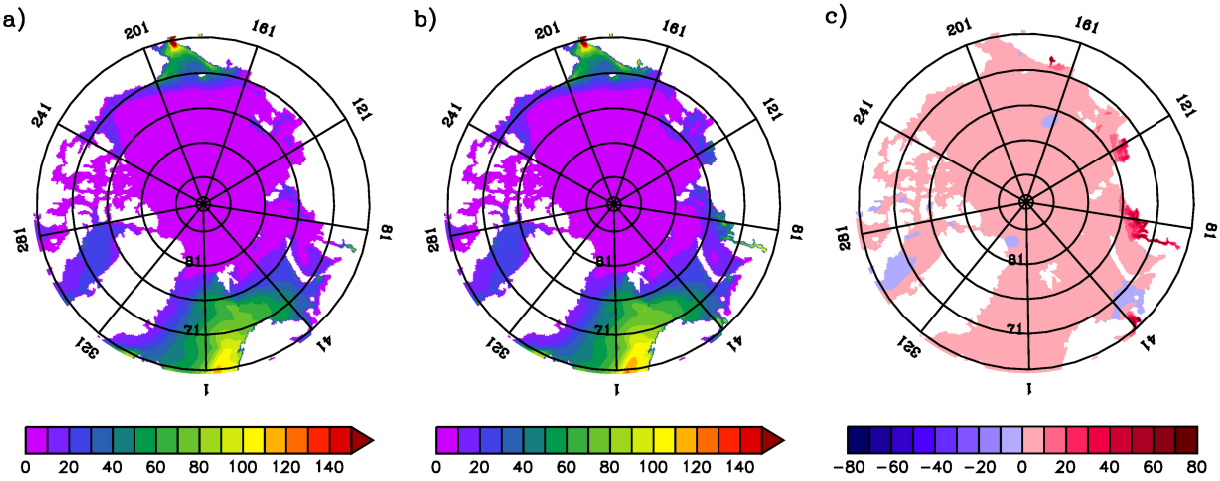
a)
b)
c)
201
161
121
81
41
1
321
281
241
71
91
0 20 40 60 80 100 120 140
0 20 40 60 80 100 120 140
−80 −60 −40 −20 0 20 40 60 80

Figure 2.

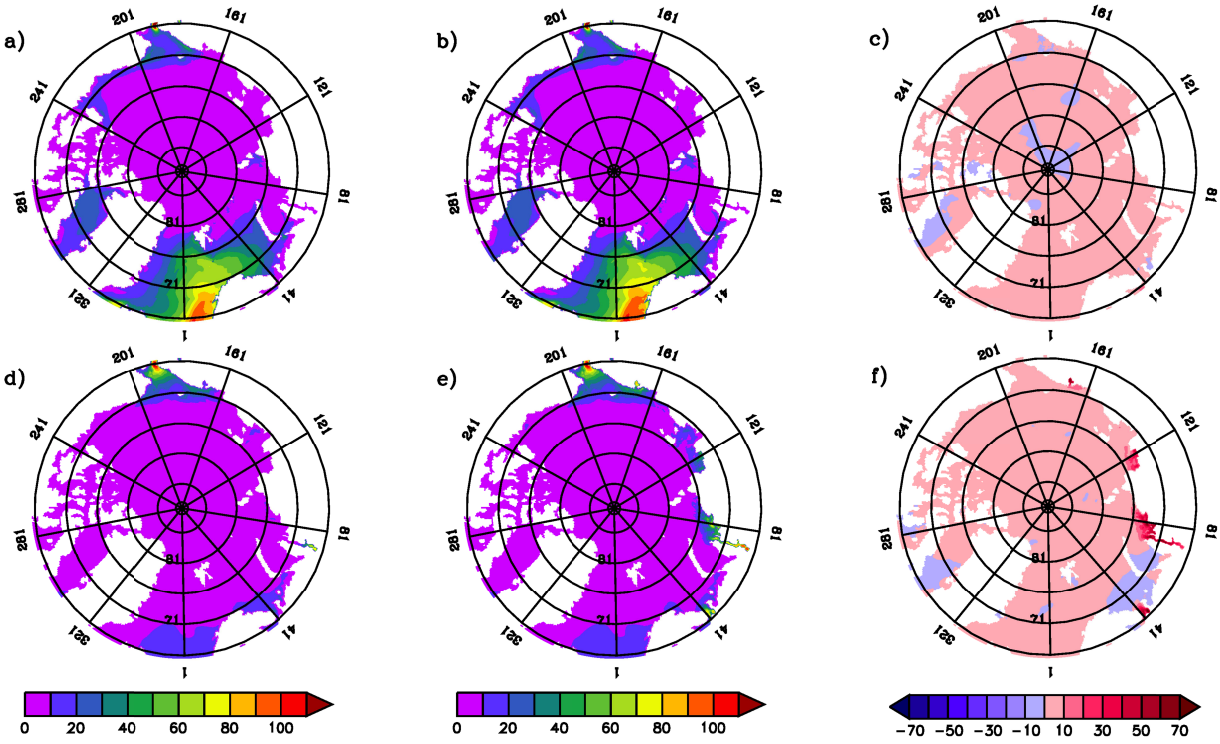
a)
b)
c)
d)
e)
f)
1
21
41
61
81
101
121
141
161
181
201
221
241
261
281
301
321
0 20 40 60 80 100
−70 −50 −30 −10 10 30 50 70

Figure 3.

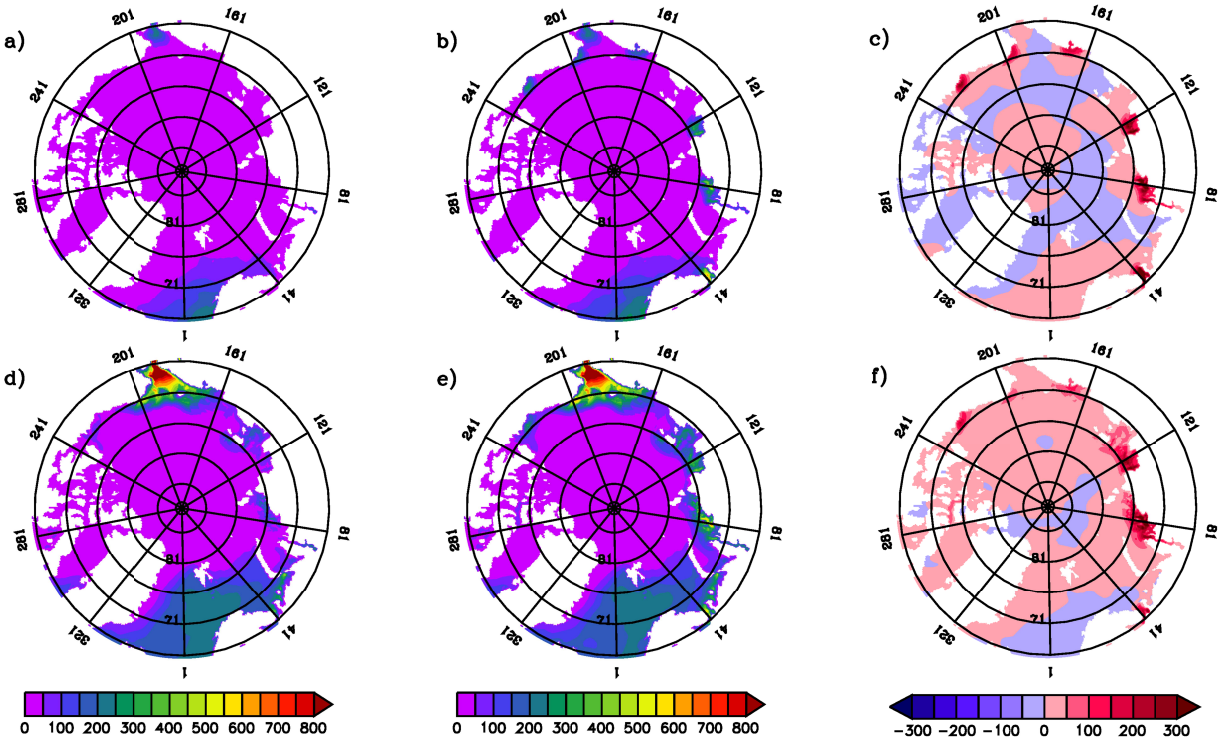
a)
b)
c)
d)
e)
f)
1
21
41
61
81
101
121
141
161
181
201
221
241
261
281
301
321
341
0 100 200 300 400 500 600 700 800
0 100 200 300 400 500 600 700 800
−300 −200 −100 0 100 200 300

Figure 4.

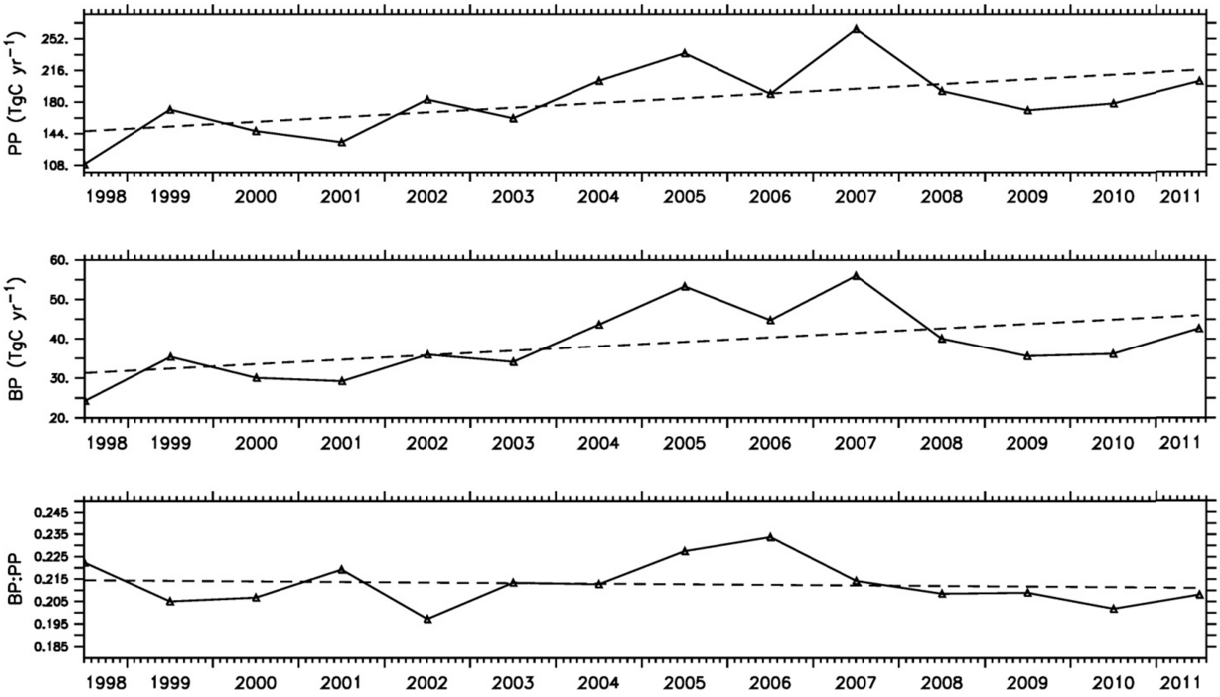
PP (TgC yr^{-1})
252.
216.
180.
144.
108.
1998 1999 2000 2001 2002 2003 2004 2005 2006 2007 2008 2009 2010 2011
BP (TgC yr^{-1})
60.
50.
40.
30.
20.
1998 1999 2000 2001 2002 2003 2004 2005 2006 2007 2008 2009 2010 2011
BP:PP
0.245
0.235
0.225
0.215
0.205
0.195
0.185
1998 1999 2000 2001 2002 2003 2004 2005 2006 2007 2008 2009 2010 2011

Figure 5.